UiT The Arctic University of Norway

Department of Arctic and Marine Biology

Senescence and nutrients in the High Arctic

Aksana Isaeva

Master's thesis in Biology, BIO-3950, August 2023

Master of Science in Biology, Northern Populations and Ecosystems,
Department of Arctic and Marine Biology, UiT – The Arctic University of Norway

Aksana Isaeva
ois004@post.uit.no

SUPERVISORS

Elisabeth Cooper
elisabeth.cooper@uit.no
Northern populations and ecosystems research group
UiT – The Arctic University of Norway

Lennart Nilsen
lennart.nilsen@uit.no
Northern populations and ecosystems research group
UiT – The Arctic University of Norway

SPONSORS

Forskningsrådet

UiT Norges arktiske universitet

FRONT PAGE

Clouds over Adventdalen, July 2022

Acknowledgements

Takk til mine veiledere, Elisabeth Cooper og Lennart Nilsen for prosjektidé, ekspertise og tilrettelegging – samt muligheten til å gjennomføre mastergraden min med feltarbeid på Svalbard.

Takk til feltassistent, Karolina B. Nilsen, for tre fantastiske uker på tundraen.

Takk til Saga og Reinhard ved UiT. Takk til Sissel og Hanna på lab (UiT). Takk til Stein Rune ved NORCE. Takk til Forskningsrådet.

Spesiell takk til Samskipnaden Svalbard, Arctic Autorent, Pole Position Longyearbyen, og Longyear 78° for kundeservice og assistanse langt over forventet nivå.

Takk til J, M, A, B og S.

Og sist, men ikke minst – en stor takk til familien for støtte gjennom et ukonvensjonelt studieforløp.

Table of Contents

Abstract

The effects of climate change on vegetation patterns toward at the end of the growing season in autumn is not yet fully understood. In addition to established light and temperature cues, other environmental factors may play a role in inducing senescence in deciduous plants on the High Arctic tundra of Adventdalen, Svalbard – such as increased access to water and nutrients. Areas with deeper snow tend to have moister and more nutrient rich soils for much of the growing season and have been observed to enter senescence later. This project aimed to test these observations and analyse whether senescence delay is a consequence of delay in snowmelt, or due to an aspect of increased water, or added nutrients.

Images taken by a landscape camera in 2019 were analysed to assess the relationship between late snowmelt and senescence length. Experimental plots were manipulated with water and water + nutrient additions on Svalbard during the growing season of 2022, whereupon RGB images, NDVI sensor data, and exploratory variables were collected.

Areas with naturally enhanced moisture and nutrients showed a strong, almost significant delay in onset and development of senescence. Day of year of active snowmelt and maximum greenness value were positively, significantly but weakly related. Plots with experimentally enhanced moisture and nutrients showed no unified trend in delay of senescence and responded to nutrient and water addition on a site/vegetation type-level. The plot experiment would however benefit from being repeated, as the sample size was here was very small, and thus not very powerful. Plant senescence did not happen later for snow accumulated plots. The growing season was instead significantly shortened.

-

Key words: climate change, growing season, senescence, water, nutrients, near remote sensing, vegetation indices, spectral senescence modelling, High Arctic, Svalbard

1 Introduction

1.1 Senescence and nutrient availability in the High Arctic

In plants, senescence is the programmed death of cells, organs, or organisms, triggered by a combination of environmental and internal cues. The understanding of senescence cues and the process of leaf browning and abscission in deciduous plants is a work in progress (Sarwat 2017; Zhao et al. 2018). In one species (*Arabidopsis thaliana*), more than 3000 senescence-associated genes have so far been found to play a role in the processes (Zhao et al. 2018). Furthermore, studies consistently show that abiotic growth conditions such as day length, light quality, humidity, and soil type have significant impact on the onset of senescence (Zhao et al. 2018) – a find that is highly relevant for plants in the communities native to the unique climatic conditions of the High Arctic.

In the Arctic, the timing of senescence in autumn is of vital importance to the local ecosystems (Cooper 2014). The growing season is short, and when the sun sets on the Arctic desert, temperatures drop fast. Plants that senesce too early lose the opportunity for additional carbon uptake during the end of the summer/beginning of autumn. Plants that senesce too late may lose valuable nutrients from the apoptotic processes, as well as the development of cold-hardiness needed to survive the adversity of winter.

Senescence timing affects the quality and availability of forage for herbivores like reindeer and geese. It also impacts the tundra carbon balance: continued warm temperatures in autumn after senescence has occurred, increase the efflux of CO_2 into the atmosphere (Uchida et al. 2010).

1.1.1 Climate change

The effects climate change will have on Arctic plant phenology during the end of the growing season is currently under debate (Cooper 2014). Along with established light and temperature cues (Marchand et al. 2004; Semenchuk et al. 2016), other environmental factors may play a role in inducing senescence in deciduous plants, such as access to water or an increase in available nutrients.

Areas on Svalbard with increased snow accumulation during winter – such as stream gullies or experimentally created snow beds (Semenchuk et al. 2015; Mörsdorf et al. 2019; Moriana-Armendariz et al. 2022) – show a tendency towards having moister and more nutrient-rich soils for much of the growing season, as well as warmer cold-season temperatures in the soil (Semenchuk et al. 2015). In addition to increased H_2O-access, the presence of water in the soil facilitates nutrient uptake in Arctic plants, promoting productivity (Chopin et al. 1998; Semenchuk et al. 2015; Mörsdorf et al. 2019). Semenchuk et al. (2015) showed that increased concentration of N and chlorophyll in leaves indicated a potential for increased growth and C-uptake, a claim supported by an increase in leaf size for some of the studied species. For *Bistorta vivipara*, treatment resulted in larger leaf size for snow-treated plants in one of the two locations. For *Luzula arcuata*, leaf size increased in treated plots in one location, but decreased in the other. *Salix polaris* showed no significant change in either location (Semenchuk et al. 2015). This indicates that response to winter insulation and increased moisture during the growing season may be both vegetation type- and species-specific.

Observationally, areas with deeper snow during winter also seem to experience a later onset of plant senescence in autumn (Cooper and Nilsen, unpublished observations).

1.1.2 Increased nutrient availability

This study is the first of its kind done in the High Arctic on Svalbard. In the absence of literature on the subject, I have reviewed the effects of increased nutrient availability on Arctic plant physiology.

In a largely nutrient-poor Arctic environment, bird cliffs on Svalbard are rare, naturally nitrogen-rich 'oases'. Bird colonies living on these cliffs transport nitrogen from the sea onto land through guano deposits during early season nesting activities. Rainfall then redistributes the organic matter downslope, creating natural nutrient gradients (Odasz 1994). Nitrogen in the arctic soil exist mostly in the form of ammonium (NH_4+), or to a lesser amount as nitrate (NO_3-). To utilize nitrate, plants need to be able to perform nitrate reduction. The plants growing in bird cliff areas grow in a gradient corresponding to available N in the soil, with maximum levels of leaf nitrate reductase activity decreasing downhill towards the coast (Odasz 1994).

In addition to nitrogen, guano supply enhances soil conductivity, potassium (K+), and phosphate (PO_4^{3-}) ion concentrations, which leads to reduced pH values (Zwolicki et al. 2012). Planktivore colonies of little auks (*Alle alle*) and piscivore colonies of Brünnich's guillemot (*Uria lomvia*) or kittiwakes (*Rissa tridactyla*) affect their adjacent escarpment in different ways, with guano deposition and ion content in the soil decreasing more rapidly with distance downslope from the piscivore colony, than the planktivore colony (Zwolicki et al. 2012).

Due to naturally low levels, nitrogen and phosphorous are co-limiting growth factors for plants in the Arctic biome (Gordon et al. 2001). Even a small increase in available nitrogen through fertilisation is enough to affect Arctic ecosystem structure and function (Arens et al. 2008). Interactions between total amount of nutrients in the environment and the rate of nutrient cycling determine nutrient availability (Klokk & Rønning 1987). Adding nitrogen alone depletes available phosphorous and releases carbon from the soil through an increase in decomposition (Street et al. 2017). Without phosphorous, the system becomes N-saturated and positive effects of fertilisation taper off. With added phosphorous, the ecosystem is released from N-saturation, and dramatically increases photosynthesis and respiration (Arens et al. 2008). In mosses, N and P in combination have been found to co-stimulate productivity and increase organic matter accumulation in the soil: the addition of both nutrients leads to a more balanced relationship between production and decomposition. Increased levels of both N and P lets carbon accumulate in the soil – where N alone leads to carbon release into the atmosphere (Street et al. 2017). Phosphorous availability thus constrains nitrogen utilisation in plants and contributes to increased CO_2 deposition in Arctic soils. Potassium levels in the Arctic are assumed to be sufficient for optimum growth, but a positive response to potassium fertilisation has been observed (Klokk & Rønning 1987).

1.1.3 Effects on plant physiology and ecosystems

As supplemental nutrients from fertilisation experiments on the Arctic tundra pass through Arctic ecosystems, several patterns emerge. Studies have shown that response to fertilisers is highly species-specific (Klokk & Rønning 1987; Gordon et al. 2001; Klanderud 2008), and not necessarily uniform for larger functional groups.

While flower production, fertility, and growth rates of shoots in vascular plant species respond positively to NPK (nitrogen, phosphorous, potassium) fertilisation (Bigger & Oechel 1982; Klokk & Rønning 1987), added nutrients depresses their photosynthetic activity (Bigger & Oechel 1982). Svalbard tundra's staple dwarf shrub species, *Dryas octopetala*, *Cassiope tetragona*, and *Salix polaris* differ in their ability to respond to increased nitrogen and phosphorous, with *Cassiope* responding most conservatively, *Dryas* having an intermediate response, and *Salix* being the most responsive (Baddeley et al. 1994). Photosynthesis in bryophytes is stimulated with fertilisation – increasing with fertiliser amount (Bigger & Oechel 1982). Like with vascular plants, bryophyte response to added nutrients differs on a species-level (Gordon et al. 2001). Nitrogen-fertilisation has also been shown to decrease lichen cover (Gordon et al. 2001).

The immediate effect of added nutrients on bare soil in the tundra favours bryophytes, which establish and increase rapidly following increased nutrient availability (Klokk & Rønning 1987; Neby et al. 2021). Compared to reference plots with 32% bryophyte coverage (vs. 66% vascular plants), restoration plots treated with fertiliser resulted in vegetation with 62% bryophytes (vs. 38% vascular plant species) (Neby et al. 2021).

Long term increase in nutrient access on the Arctic tundra leads to changes in ecosystem composition. A study done in Ny Ålesund, Svalbard between 1991 and 1995 showed that over time, the amount of *Dryas octopetala* and *Saxifraga oppositifolia* at the sites decreased, while bryophytes, *Salix polaris* and *Polygonum viviparum* increased (Robinson et al. 1998). There was a change in the amount of plant cover, with bare ground decreasing over time, and dead vegetation accumulating, while living material decreased in comparison (Robinson et al. 1998). Bryophyte communities may also experience a change in species composition as a result of phosphorus and nitrogen fertilisation (Gordon et al. 2001).

Experimental increase in temperature in addition to NPK-fertilisation resulted in significant composition changes in the plant community. Tall grasses (*Festuca* spp., *Poa alpina*) and forbs (e.g., *Cerastium alpinum*, *Potentilla crantzii*) increased in numbers over time with added fertilisation, and especially when treated with fertilisation + warming. Smaller forbs (e.g., *Tofieldia pusilla*), one lycophyte (*Selaginella selaginoides*), and most bryophytes and lichens decreased in numbers. After a total of four years of warming + fertilisation treatment, 57% of mosses, 57% of liverworts and 44% of lichens had vanished completely (Klanderud 2008).

Fertilisation in combination with warming thus looks to be the most potent treatment when it comes to facilitating ecosystem-wide composition changes. The effects of nutrient increase seem to be highly persistent, and vegetational response to heightened net mineralisation from soil warming will depend on the rate at which nitrogen and phosphorous availability increases (Gordon et al. 2001).

1.2 Effects of nutrients on senescence elsewhere

As is the case for the Arctic, the impact of nutrients on senescence elsewhere is not broadly studied. However, there is a small accumulation of evidence towards nutrient addition prolonging the growing season, and postponing senescence in deciduous trees (Thomas & Ahlers 1999; Schaberg et al. 2003; Sigurdsson 2011; Fu et al. 2019). One study also found that when deciduous trees were intensely fertilised in late autumn, they kept their green leaves until temperatures sank to below 0°C (Sakai & Larcher 1987, as cited in Fu et al. 2019).

Added nitrogen to saplings of horse chestnut (*Aesculus hippocastanum*) and beech (*Fagus sylvatica*) showed that an increase in nitrogen delayed the onset of senescence for both species (Fu et al. 2019). However, in relation with leaf-out, the effect was strongest on horse chestnut: late bloomers stayed green longer than early bloomers. In beech, nitrogen had a weak effect on late bloomers, with early bloomers staying green longer into the fall (Fu et al. 2019).

1.3 Near-Remote-Sensing

Near-Remote-Sensing (NRS) provides a low-cost, low-maintenance technique to monitor changes in vegetation beyond the capabilities of remote sensing (Tømmervik et al. 2014; Permentier et al. 2021). In the Arctic, the best options for gathering NDVI-information are near-surface sensors and UAS (Tømmervik et al. 2014).

Digital cameras have successfully been applied to observe seasonal plant patterns (Richardson et al. 2009; Anderson et al. 2016; Westergaard-Nielsen et al. 2017), while also recording information on the productivity of the observed vegetation in the form of ‘greenness’ (Westergaard-Nielsen et al. 2017).

Although broadly used (e.g., Engstrom et al. 2008, Anderson et al. 2016, Parmentier et al. 2021), NDVI is not ideal for end of season observations. There is still disparity between what is observable by eye and what can be interpreted through NRS. Understanding is lacking for both processes, as well as whether the data coming of out these sensors is a good indication of what is going on.

The use of remote sensing via satellites in monitoring autumnal senescence is difficult on Svalbard due to cloudy, overcast weather year-round with long stretches between clear-sky images. Climate change promises an increase in annual precipitation, further intensifying the issue.

1.4 Aims

The aim of this study is to test the following hypotheses:

1. Areas with naturally and experimentally enhanced moisture and nutrients show delayed onset and development of senescence.
2. The addition of water and nutrients delays the onset and development of senescence and prolongs the growing season in nutrient-limited plant communities of Adventdalen, Svalbard.

The primary focus of the study is to explore the previously unexplored relationship between nutrients and the onset of senescence in autumn. It also aims to answer the questions of whether plant senescence happens later in landscape depressions where snow tend to accumulate, as well as if the season is longer in these depressions than in the other areas? Or does the growing season simply shift to start and end later? Additionally, I will briefly address the use of NRS equipment in the field for use in the study of autumnal senescence.

Hopefully, results from this project will enable scientists to better understand and predict the potential consequences and effects of climate change on the High Arctic plant communities.

2 Study area

2.1 Location

The study area lies in Adventdalen, Spitsbergen (78°10'N, 16°04'E), in the Svalbard archipelago, Norway. Adventdalen valley is approximately 30 km long and between 3 and 4 km wide. At its centre runs the broad, braided river Adventelva, into which several smaller rivers such as Todalselva, Bolterelva, and Foxelva converge. The primary field area with camera rack plots #1 (*Dryas*) and #2 (Graminoids) were placed about 15-20 km from Longyearbyen, and about 5 km east of the end of the road below Gruve 7, in the direction of Jansonhaugen. The secondary field area with camera rack plots #3 (*Salix*) was located some 10 km closer to town, on the southwestern side of the road at Braathensletta, between the road and the river Endalselva. The landscape camera was placed on the mountainside of the mountain Breinosa, below Gruve 7, overlooking the valley in a north-western direction. For details on the placement of the landscape camera, see Parmentier et al. (2021), "Breinosa".

In Longyearbyen, polar day starts around the 20th of April and lasts until around the 21st of August each year. Polar night begins around the 26th of October and ends around the 16th of February (Barr 2022). This results in a compressed growing season, here defined as June, July, and August.

Svalbard lies north of the polar front and has a characteristic maritime High Arctic climate: it is cold, dry, cloudy, and occasionally foggy in Adventdalen. Readings from the closest weather station, Svalbard airport Longyear, show a mean annual temperature of -4.7°C, and a mean monthly growing season temperature of 5.1°C (last 50 years – 1972-2021, Svalbard Lufthavn, https://seklima.met.no/). Mean annual precipitation at the same station during the same period was 206 mm, with most of the precipitation falling during the winter months, September to March, as snow (https://seklima.met.no/).

Adventdalens dryness is further exacerbated by local wind conditions in the valley. Mean average monthly wind strength measured at Longyear airport between 1975 and 2021 was 5.0 m/s (seklima.met.no), with highest measured average monthly wind strength at 30.4 m/s (11.1985, seklima.met.no). The main wind direction in Adventdalen is from the south-eastern valley basin, and out in the north-western direction towards the sea.

2.1.1 Location maps

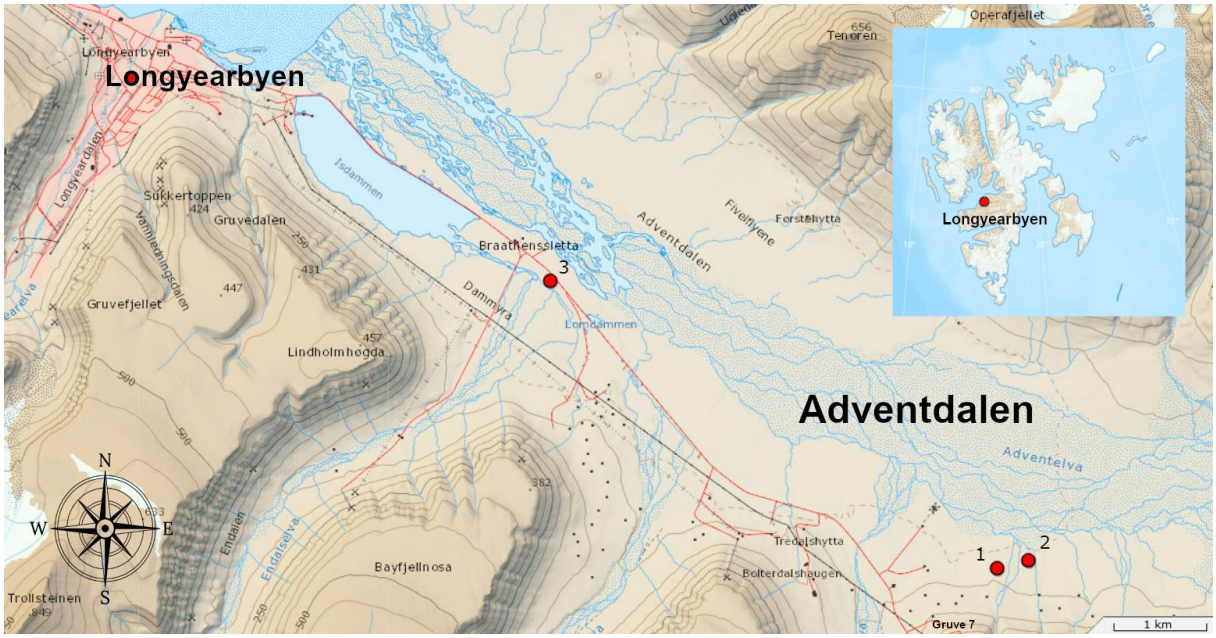

Figure 2.1: Map of Adventdalen in relations to Longyearbyen and a mini map of Svalbard (sans Bjørnøya), with the experimental study sites marked: #1 and #2 by Gruve 7, and #3 by Braathensletta. Maps © Norsk Polarinstitutt (https://toposvalbard.npolar.no).

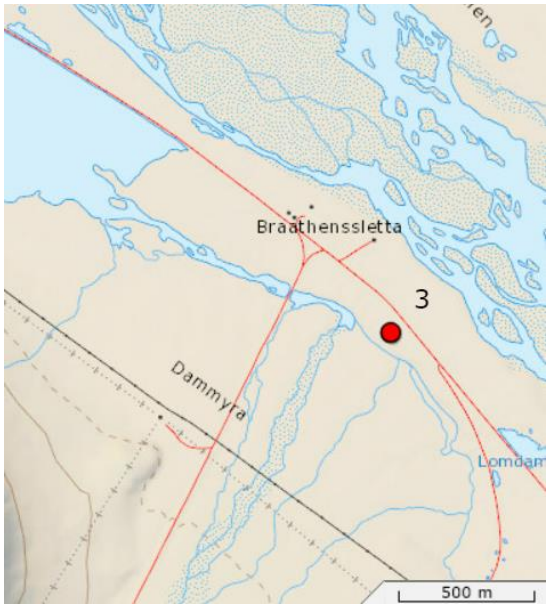

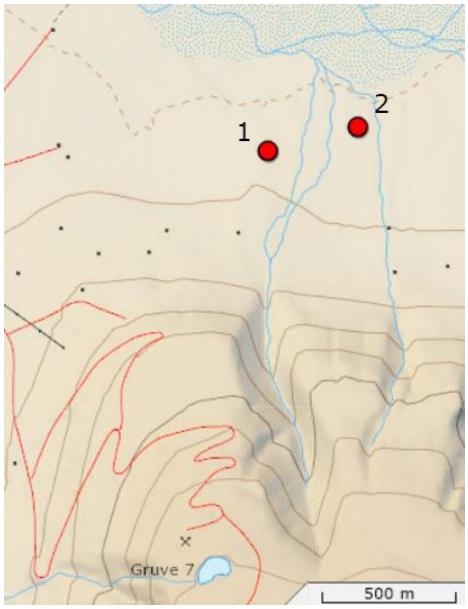

Figure 2.2A + **2.2B**: Closeup-maps showing the locations of the experimental study sites: #1 and #2 by Gruve 7, and #3 by Braathensletta. Maps © Norsk Polarinstitutt (https://toposvalbard.npolar.no)

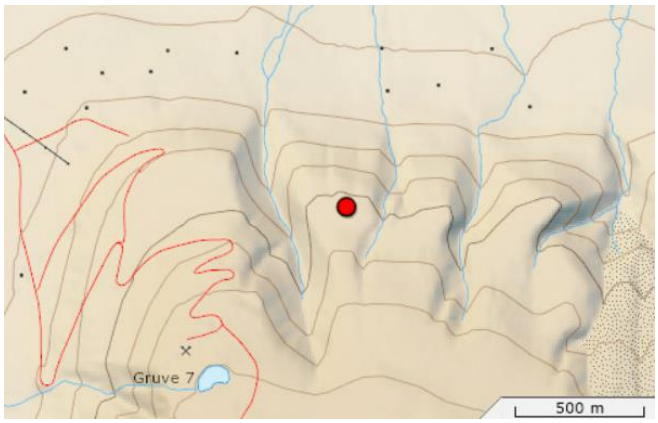

Figure 2.3: Map illustrating the approximate placement of the landscape camera, on the mountain ridge below Gruve 7. Map © Norsk Polarinstitutt (https://toposvalbard.npolar.no)

Figure 2.1 and 2.2A+B show the placement of the experimental plots in Adventdalen. Figure 2.3 is an illustration of the approximate location of the landscape camera in relation to Gruve 7 (ref. Parmentier et al. 2021).

2.2 Geology and deglaciation

Adventdalen is a deglaciated river valley that was formed through deglaciation during late Quaternary period, and the following lowering in sea-levels throughout the more recent Holocene epoch (Mangerud et al 1998; Lønne & Nemec 2004; Lønne 2005). The underlying soil remains in a permanently frozen state, with local permafrost on Spitsbergen being dated to be 2364 years of age (today - after Hansen et al. 2007). Maximum active soil layer thickness lies between 106 and 130 cm, depending on associated snow regime and vegetation type (Xu et al. 2021).

The soil profile in the study area is mainly mineral, with a thin organic soil layer. Soil on Spitsbergen is slightly acidic with a pH ranging between 5.0 and 6.5 downward through the soil profile (Strebel et al. 2010).

The study area's main water supply outside of precipitation comes from glacial runoff through creeks and rivers, with slowly moving water creating marsh-like conditions in some areas on its way downslope. Permafrost melt also supplies moisture to the area, from

underground. Water is thus continuously supplied to the area throughout the growing season (Elvebakk 2005; Morgner et al., 2010). Some riverbanks and river terraces in the study area show disturbance made by cryoturbation.

2.3 Flora

Adventdalen lies within the Arctic tundra biome, subzone A-B (Walker et al. 2005), where vegetation is characteristically sparce, with the few plant species present rarely growing above 10 cm in height. Most of the vegetation in the valley can be found between the banks of Adventelva river and the steep sides of the surrounding mountains.

Local vegetative communities can be roughly divided into heaths and mesic meadows (Elvebakk 2005). Heaths reside closer to the mountains on ridges with stony, well-drained soil (Elvebakk 2005; Morgner et al. 2010). The meadows lie further away from the valley sides on flat river terraces with finer mesic substrates from fluvial deposits. A mesic meadow soil profile of the area showed an 0.2-6.0 cm thick upper O-horizon containing small roots and decomposing plant matter on top, a 1-5 cm thick dark brown A-horizon below, and a B/C-horizon of grey silt underneath (Strebel et al. 2010). A wetter area of mesic meadows has been measured to have an 1-7 cm thick organic peat horizon (H-horizon) containing poorly decomposed organic matter, followed by a 3-9 cm thick grey A-horizon of decomposing organic matter atop a grey-blue B/C horizon (Strebel et al. 2010). The H-horizon in this wetter area was water-saturated throughout the growing season (Strebel et al. 2010). Plant roots have been found down to a depth of 45 cm (Strebel et al. 2010). Registered pH in the area was at 6.1 for heaths and 5.7 for meadows (Semenchuk et al. 2015).

Plant species in the vegetative communities are overall similar, but dominant species and amounts of vegetation cover differ. Heaths are dominated by the following vascular plants: *Cassiope tetragona, Dryas octopetala*, *Salix polaris, Saxifraga oppositifolia*, *Alopecurus borealis* and *Bistorta vivipara* (Cooper et al. 2011). Mesic meadows are dominated by vascular *Salix polaris*, *Luzula confusa*, *Alopecurus magellanicus, Dryas octopetala* and *Bistorta vivipara* (Morgner et al. 2010; Cooper et al. 2011). Other species found commonly in the study area are *Oxyria digyna, Stellaria longipes, Pedicularis hirsuta,* and *Equisetum arvense*.

Bryophytes are more commonly found in mesic meadows over heaths, accounting for up to 50% of the plant cover in some areas. Common bryophyte species include *Sanionia uncinata*, *Tomentypnum nitens*, *Polytrichum* spp., *Dicranum* spp., and *Distichium* spp. (Cooper et al. 2019).

Adventdalen is home to over 20 different species of lichens, with the families *Lecidea* and *Polyblastia* presenting several variants (Øvstedal et al. 2009). Additionally, there are three lichen species that so far have only been found in Adventdalen: *Buellia concinna*, *Buellia geophila*, *Placynthiella uliginosa* (Øvstedal et al. 2009).

2.4 Fauna

Staple terrestrial herbivores found in the area are the Svalbard reindeer (*Rangifer tarandus platyrhynchus),* and the Svalbard rock ptarmigan (*Lagopus muta hyperborea*). In the summer month breeding season, the coastal Longyearbyen-area also hosts the migratory geese *Anser brachyrhynchus* and *Branta leucopsis*. Local omnivores that occasionally feed on plants (berries, seeds e.g.) are the Arctic fox (*Vulpes lagopus*) and the Snow bunting (*Plectrophenax nivalis*). The Arctic skua (*Stercocarius parasiticus*) can also be found inland, as far up as the study area, during the breeding season.

While the reindeer in Adventdalen don't exude regulatory pressure on Svalbard flora, their feeding habits provide selective pressure on different vegetation types, preferring to graze on the grass *Alopecurus borealis* over the graminoid *Luzula arcuata*, or the dwarf shrubs *Salix polaris* and *Cassiope tetragona* (Wegener & Odasz-Albrigtsen 1998). In large parts of the Arctic, reindeer have been found to indirectly reduce shrub abundance and increase nitrogen in the soil (Sundqvist et al. 2019). Reindeer and ptarmigan have also been found to co-feed on the flora in the study area, albeit in winter: ptarmigans search for food in feeding craters excavated by reindeer (Pedersen et al. 2006).

2.5 History of anthropogenic activity

Svalbard became an official part of Norway in the 1920s, following the signing of the Svalbard Treaty in February 1920 (Arlov 2003, p. 294-305). The main anthropogenic activity

in the Norwegian Adventdalen area has traditionally been coal mining. Since the beginning of the new millennium, coal mining has decreased drastically, and Longyearbyen entered a post-industrial aera where the new "industry" has become scientific research (Arlov 2003, p. 462). A century post-Treaty, scientific endeavours flourish as never before: As of August 2023, there are currently more than 40 active ongoing projects taking place in Adventdalen, and over 600 on Svalbard in total (https://researchinsvalbard.no). Additionally, and especially in winter, Longyearbyen is an attractive tourist destination, numbering in around 30 000 visitors per year (https://svalbardmuseum.no/).

Globally, the last 25 years have been the most influential on the High Arctic climate of the Anthropocene. During the last 25 years, 1997 to 2021, global anthropogenic activity has brought Adventdalen (as measured by Longyear airport) an increase in temperature of +2.4ºC (+1.0%) – from compared to the mean annual temperature from the years 1922-1946 of –5.8°C (https://seklima.met.no/). The mean annual temperature in the area for the last 25 years, 1997-2021, was –3.4°C (https://seklima.met.no/). The temperature increase has been largest in the winter months, as the change in growing season temperature between 1922-1946 (4.4°C) and 1997-2021 (5.7°C) was "only" +1.3°C, or +0.5% (https://seklima.met.no/). The change in temperature has not been gradual, as mean annual temperatures for the 75 years 1922-1996 were –6°C, and mean annual growing temperatures were 4.3°C (https://seklima.met.no/).

Mean annual and monthly growing season precipitation in Adventdalen has also increased. Here, the change has been more gradual, with less of a clear pattern for the last 25 years. Mean annual precipitation in 1997-2021 was 213.6 mm and mean monthly growing season precipitation was 16.9 mm (https://seklima.met.no/). This is an annual precipitation increase of +46.8 mm (+28, %) since 1922-1946's annual 166.8 mm/year, and a +4.4 mm (+35 %) increase since 1922-1946's mean monthly growing season precipitation of 12.5 mm (https://seklima.met.no/).

3 Materials and methods

3.1 Study design

This project consisted of two parts:

1. Analysis of image data from a landscape camera set up in previous years for an ongoing UiT project collaboration (see Parmentier et al. 2021).
2. Analysis of image data from 9 camera rack plots (hereafter - plots) established specifically for this thesis in 2022.

The landscape camera was placed on the mountain Breinosa, to provide large-scale coverage to more detailed image data from camera racks in the valley below (Parmentier et al. 2021). For more details on this study, see Parmentier et al. (2021). The image data used for this project was taken in the year 2019.

Field work related to the plots was carried out in June, July, and September of 2022.

3.2 Experimental setup

3.2.1 Plot selection

Three study sites were established in three separate areas, near existing NRS-equipment for an ongoing UiT project collaboration, with the goal to monitor and study the response of three distinct vegetation types to nutrient addition.

Site #1 was established on the slope of a rocky heath, dominated by the dwarf shrub *Dryas octopetala*. Site #2 was on a flatter, wet, mesic meadow dominated by graminoids (*Dupontia fisheri* and *Eriophorum scheuchzeri*). And Site #3 was on another heath, a flat area dominated by the dwarf shrub *Salix polaris*.

A total of nine camera rack plots were established upon arrival in Adventdalen, three for each vegetation type: one control plot (C), one water addition plot (W), and one nutrient addition plot (N) at each site. The cameras and NDVI-sensors were mounted on a wooden frame at a height of approximately 133 cm, facing down at a 90º angle. Underneath them, plots measuring 1x1 m were sectioned off with minimally invasive equipment: metal tent plugs and

nails in the corners, with white thread drawn between them. The racks were also equipped with loggers registering temperature and soil moisture through sensors buried at a depth of 10-15 cm near the foot of the racks, close to the plots but not disturbing them.

The placement of the plots at the study sites were based on the following criteria: Relatively flat topography. Approximately similar vegetation coverage. Distance of several meters away from each other. Plots had to be at a reasonable distance from each other, as not to accidentally affect one another. This led to only control plots, which would remain untouched, being established up-hill from the rest of the other plots at Site #1 and #2. Additionally, an absence of large stones was favoured at Site #1. Treatments – control (C), water (W) and nutrients (N) – were assigned at random. The coordinates for each plot can be found in the Appendix, in table. T3.1. Camera racks plots are illustrated in figures 3.1A+B, 3.2, and 3.3.

Figure 3.1A + 3.1B: Pictures of established camera rack plots at Site #3 (A), and Site #2 (B). The red frame of 1x1 m was here used as a reference for placing the plots directly under the camera lens.

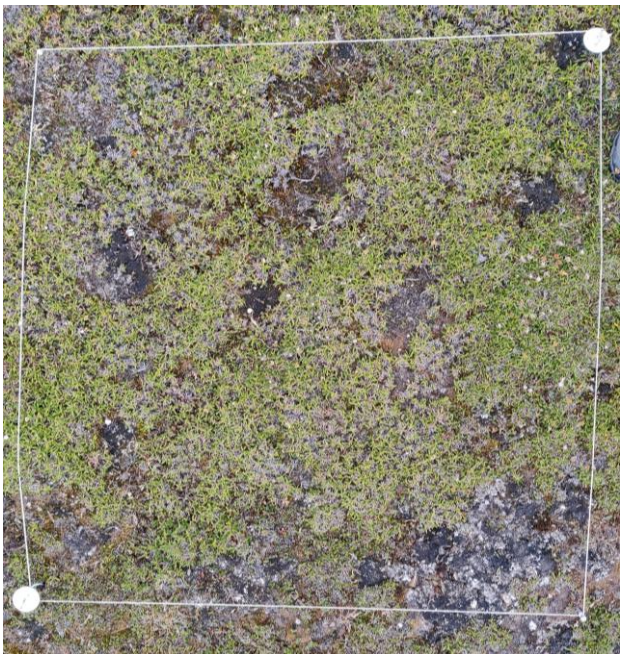

Figure 3.2: Picture of the established control plot at Site #1, C1.

Figure 3.3: Picture of the three established plots at Site #1.

The total number of camera racks was limited by the amount of equipment available from UiT. In order of establishment by site, they were C1, W1, N1, C2, W2, N2, C3, W3, N3.

3.2.2 Water and nutrient addition

Six of the established plots were manipulated by adding water (W-plots, W1-3) and water-solved nutrients (N-plots, N1-3) at intervals through the beginning of the growing season, from the end of June to mid-late July. As plants primarily take up nutrients at the beginning of

the growing season, nutrient addition and watering were compressed to the duration of the fieldwork, roughly three weeks, instead of the full growing season duration, from June to August.

Each W-plot was treated with a total of 90 L of water. This equals an approximate fivefold increase in precipitation, compared to present day values. Watering was done through a commercially available 10 L watering can (figure 3.4), with local water acquired at the study area. For Site #1 and #2 the same water supply was used, a nameless creek nicknamed 'Dobbeltbekken', which was located between the two sites (see figure 2.3B). The water supply for Site #3 came from the river Endalselva. Water plots were added to the experiment as a measure to control for water addition in adding water-solved nutrients to N-plots.

In the Arctic, too much added nutrients may lead to a reduction in individual plants and amount of vegetation cover (Forbes and Jefferies 1999; Gordon et al. 2001), as well as actively damaging plant physiology (Hussein et al. 2021) and making the soil hostile to the existing community/ecosystem (Forbes and Jefferies 1999). To avoid doing damage to the naturally nutrient poor Arctic soil, conservative amounts of fertiliser were used for this experiment.

Each N-plot received the same concentration of fertiliser. The fertiliser was applied at a total concentration of 5 g N, 2.25 g P, and 4.25 g K per plot. This, in accordance with earlier Arctic nutrient addition studies (Bigger & Oechel 1982, Baddeley et al. 1994; Robinson et al. 1998; Neby et al. 2021). It equals to a fivefold increase in N-availability compared to the estimated average Arctic N-turnover of 1 g/year, as described in Baddeley (1994). Fertiliser was dissolved in water, with each N-plot receiving 90 L of water in total.

As phosphorous (P) and nitrogen (N) are co-limited in the arctic (Street et al. 2017), to simulate increased nutrient availability, a fertiliser with an NPK ratio of 2– 0.9–1.7 was chosen to avoid N-saturation in the soil. A positive effect on vegetation by added potassium (K) has also been found by Babb (1973), as cited in Klokk & Rønning (1987).

The fertiliser used for this experiment was the commercially available Substral Hestegjødsel, from Substral Plantenæring, The Scotts Company Nordic AS, 0214 Oslo, Norway.

The remaining three control plots, C1-3, were not manipulated in any way.

Figure 3.4: Picture of the watering can with one of the buckets used for mixing fertilizer.

3.2.3 Image capturing

The landscape camera used for image capturing was the CuddeBack E2 time lapse camera (CuddeBack Digital, WI, USA). It recorded RGB (Red-Green-Blue) images in JPG format at set at set intervals of 3 hours, to a total of up to 8 images per day. However, some days had only 3-6 usable images due to poor weather conditions.

The landscape camera recorded images in the period 09.05.19-02.10.19.

To monitor the onset of senescence in the plots, two different RGB-cameras were used for image capturing: the *Browning Strike Force Pro XD BTC-5PXD* (Browning Trail Cameras, AL, USA) and *Fricam Start, Model BG523* (China). The Browning cameras were used for all plots except C2, where the Fricam camera was used.

The Browning cameras recorded images as AVI videos daily. Some of these files ended up being very large (up to 1,5 GB!) due to unknown factors, possibly wind/weather disturbance. Additionally, the Browning cameras took images in JPG format, when detecting motion. Only the N1 camera did not produce additional JPG images. The resolution for the Browning cameras was 4208 x 2368 p. The Fricam camera recorded images in JPG format at set at set intervals of 1 hour, to a total of 24 images per day. The resolution for the Fricam camera was 3264 x 2448 p.

Plot cameras recorded images in the period 30.06.22-27.09.22.

All three camera types taking RGB-images were commercially available wildlife cameras.

3.3 Exploratory variables

3.3.1 NDVI

NDVI – normalised differences vegetation index – uses near-infrared and red wavelength reflection to measure the relative amount of vegetation and vegetation vitality, by calculating vegetation greenness. As these values change with the increase and decrease in green chlorophyll, NDVI measurements provide valuable senescence information, in addition to RGB-images.

To measure the NDVI values for each plot, Decagon SRS-NDVI (Decagon Devices, WA, USA) sensors were used to measure spectral reflectance at 630 and 800 nm. They recorded values at 2-hour intervals, to a total of 12 per day. Two wavelengths were used to measure spectral reflectance at 630 nm and 800 nm, and calculated NDVI values automatically. Three of the NDVI sensors, C2, C3 and N2 registered different IR-values, and did not calculate NDVI values.

3.3.2 Soil moisture and soil temperature

Soil moisture and soil temperature data was collected by sensors attached to loggers on the rack at each plot. Decagon 5TM Soil Moisture and Temperature sensor (METER Group, WA, USA) recorded data at 2-hour intervals during each day, to a total of 12 daily measurements.

Soil moisture was recorded as volumetric water content (VWC m^3/m^3), and soil temperature was recorded in degrees Celsius (°C).

As the sensors were buried outside the plots, additional water was used to include them in the watering/nutrient efforts: each time a plot was watered/added nutrients to – the sensor patch was watered/added nutrients to.

3.3.3 Soil samples

To assess the concentration of nutrients in the soil, soil samples were taken twice during the fieldwork: once at the beginning before any nutrients had been added, and once at the end, during our last field day, once all manipulation efforts had been completed.

Samples were taken at the lower right corner just outside each of the nine plots, so as not to disturb the vegetation. We made sure to evenly apply treatment over the entirety of each plot, so that the area just outside where soil samples were taken would have received equal efforts in manipulation as the plots themselves.

3.3.4 Leaf measurements

To assess nutrient uptake in the vegetation, the leaf length of the dominant plants was measured at each plot at the end of the fieldwork. Measurements were done by hand with a transparent ruler. Leaves of *Dryas octopetala* and *Salix polaris* were measured along the midrib from base to apex on each leaf. Graminoids were measured along the stem from where it differentiated from the ground cover and to the end of the blade. The decision to not measure the width of the leaves (or the blades of graminoids) was made as leaves of *Salix polaris* at Site #3 often were bent in a U-shape. Unbending them to take measurements would have damaged the leaves.

Figure 3.5: Picture of the red square used to divide the 1x1 m plots into 4x4 squares at Site #3.

The red square previously used to establish the plots underneath the camera racks, was used to divide each plot into 4 x 4 squares of 25 x 25 cm each, as seen in figure 3.5. Within each of the five squares, five leaves were chosen at random (one in each corner, one in the middle) and measured to a total of 80 leaves per plot. For all nine plots, a total of 720 measurements were taken.

3.4 Data processing and analysis

3.4.1 Image data

3.4.1.1 Processing

Landscape camera

From the available data, one landscape image was selected per day based on the following criteria: Low contrast, avoidance of overly sunny sunlight, good solar angle (no sun facing the camera head on). Images taken at 2:56 pm consistently showed the best conditions in relation to camera angle and light, when images take at 2:56 pm couldn't be used due to adverse weather and light conditions (fog, clouds, rain, blinding sunlight etc.), other images from the same day were selected. Due to the absence of night on Svalbard in the summer, second option images ranging around the clock were used.

A total of 138 images taken from day of year (DOY) 133 (May 13th, 2019) until DOY 270 (September 27th, 2019) were used.

The images series was stabilised and cropped using the free software Hugin (2021.0.0, Pablo D'Angelo, 2022) and GIMP (2.10.34, The GIMP Development Team, 2022).

To identify areas of interest (AOIs), an image was chosen during peak growth season (DOY 215 – August 3rd, 2019), printed, and marked up by hand (figures 3.6A+B). The AOEs were organised into five regions, region A though E (figures 3.7 and 3.8A-E). Within each region large, homogenous areas of ambient greenness levels (condition 'ambient') were chosen to contrast against the marked AOIs with greener colouring (condition 'green'). Each region had up to two ambient areas, with the exception of region A, which had ended up with four. This, due to region A covering a substantial area, at great distance from the landscape camera and having a very heterogeneous greenness profile. This is also the reason for area E having two

ambient areas: distance from camera, and heterogenous greenness profile. A total of 55 AOIs were selected, including ambient areas A1, A7, A15, A17, B1, C1, D6, E2 and E8.

Figure 3.6A: Raw, aligned image from the landscape camera, taken on DOY 215.

Figure 3.6B: All areas of interest marked up and digitally imported.

The stencil was then scanned and applied to all landscape camera images, which were cropped into the selected AOIs using GIMP. Each AOI was exported as a TIFF file with a layer for each day of year.

The landscape camera did not have any days with missing images.

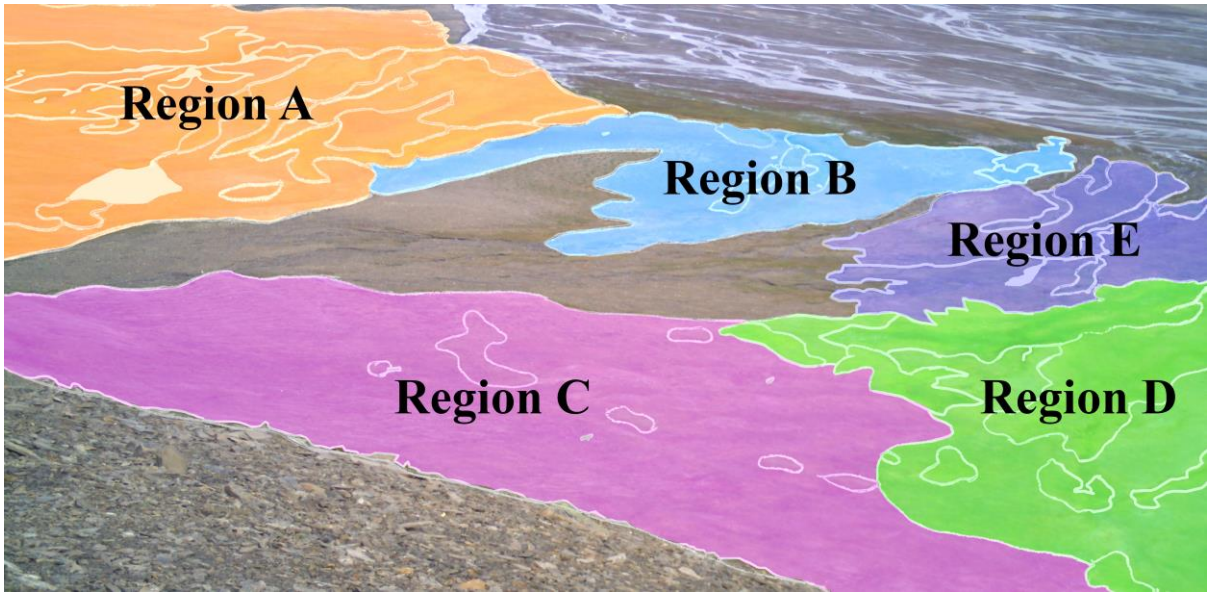

Figure 3.7: All areas of interest, divided into regions.

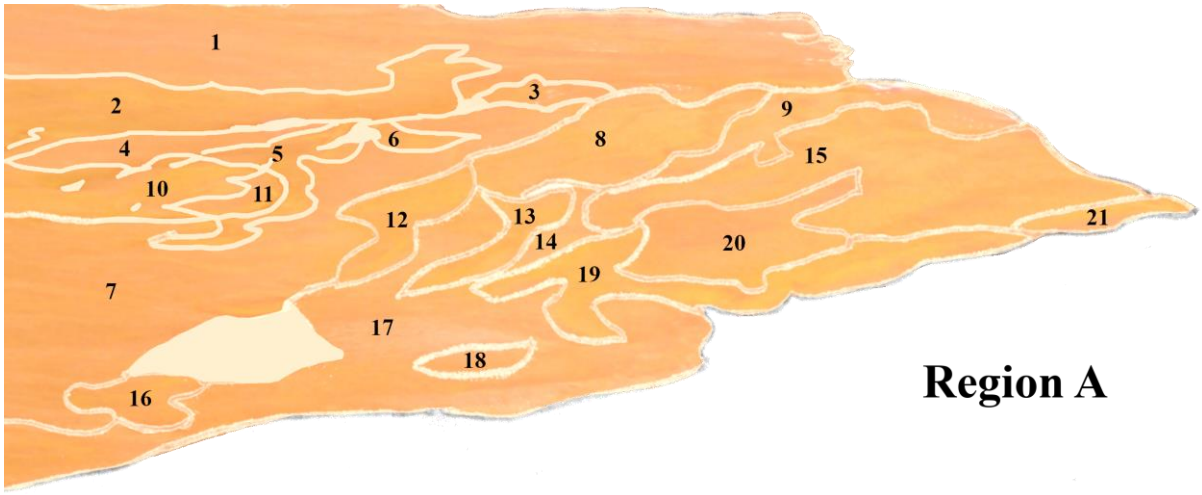

Figure 3.8A: Region A, AOIs A1-21.

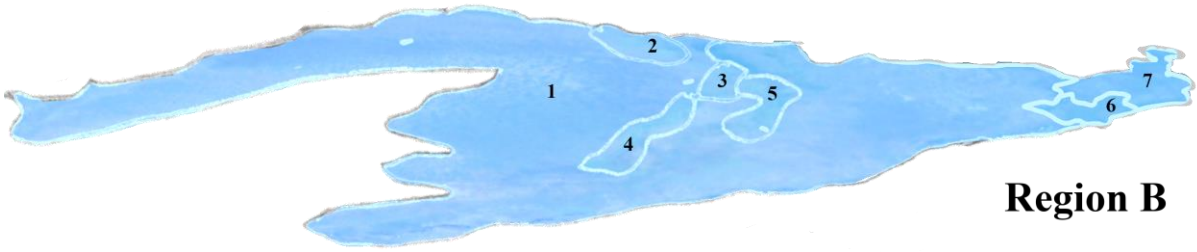

Figure 3.8B: Region B, AOIs B1-7.

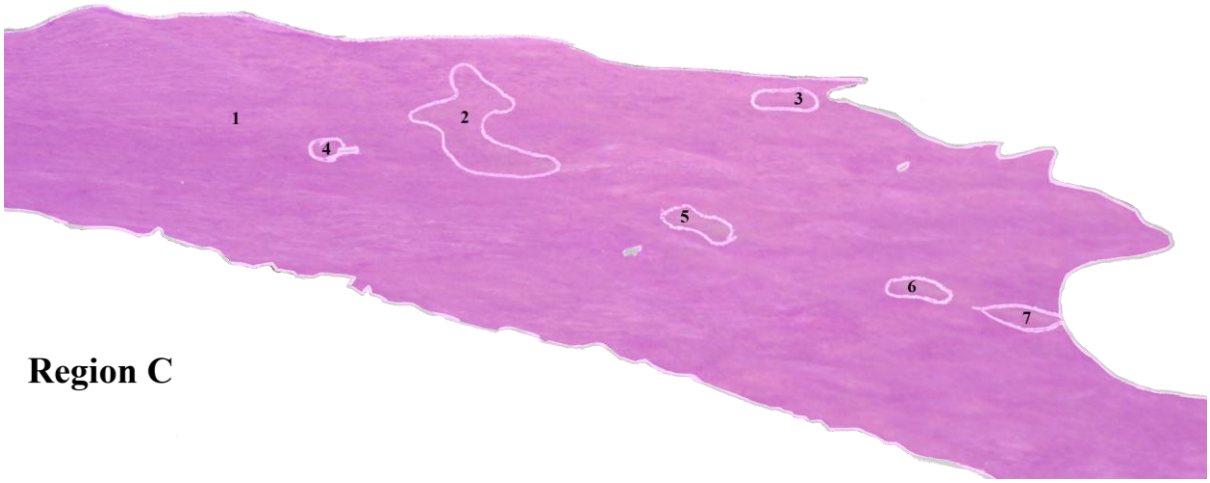

Figure 3.8C: Region C, AOIs C1-7, slightly cropped for visibility.

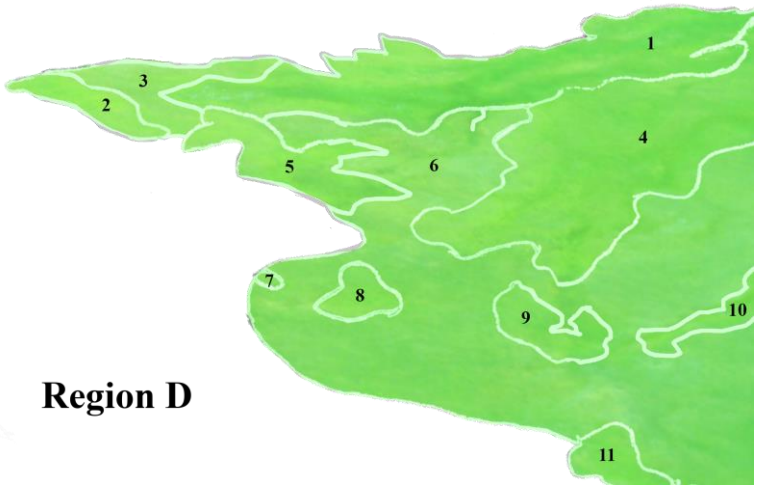

Figure 3.8D: Region D, AOIs D1-11.

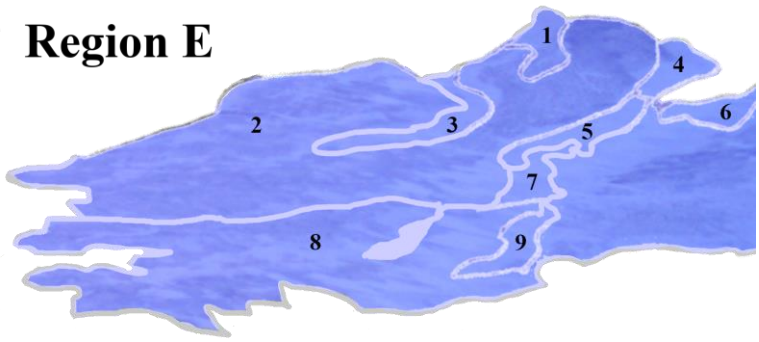

Figure 3.8E: Region E, AOIs E1-9.

Plot cameras

From the plot cameras, one image a day was selected using similar criteria as the landscape camera images: Images were chosen with the least possible amount of contrast (sun angle/clouds), no disturbing elements (shadows, animals, water). Images with higher contrasts were used in the absence of better-quality images. Screen captures from the daily video files were preferred, as images captured by the plot cameras' motion detection often were "actions shots" – wind images, animals, other movement. As the plot cameras were closer to the ground than the landscape camera, daily best images varied form plot to plot, but were usually taken between 9 am and 12 pm.

Unfortunately, the cameras were placed a little too close to the ground, and in most cases were could not include the entire 1x1 m plots in the shot. A good 80-90% of the plots were included, but only around 70% of the plots were used in the image analysis, as the shot areas "moved around" due to the effects of wind and animal presence on the camera racks: the wind is rather strong in Adventdalen, often shaking the racks, and reindeer especially are curious and have been known to use similar camera racks to the plot racks for scratching. The images required no stabilisation and were cropped using GIMP software, before being exported as TIFF files for analysis (e.g., figure 3.9).

Due to disturbances caused by wind, equipment malfunction, and animal presence, several cameras ended up with missing days. An overview of the exact dates for the missing images by plot can be found in table T3.2, in the Appendix.

Figure 3.9: Illustration of crop, here an image of plot C1 taken on the 7th of July.

A total of 75 images were used for plot analysis, taken between DOY 182, July 1st, 2022, and DOY 256, September 13th, 2022 (first snowfall of the year, lasting > 1 week).

3.4.1.2 RGB extraction + GCC calculation

Mean RGB-values were extracted from the TIFF files for each AOI and plot with the 'raster' package (v. 3.6-23, Hijmans, 2023) through RStudio (v. 421, Posit, PBC, 2023) in R (v. 4.2.3, R Core Team, 2023).

The extracted RGB-values were then used to calculate the Green Chromatic Coordinate (GCC) vegetation index using the following equation, figure 3.10:

$$GCC = \frac{G_{DN}}{R_{DN} + G_{DN} + B_{DN}}$$

Figure 3.10: GCC calculation formula. R_{DN}, G_{DN}, and B_{DN} represent the digital number of pixels in the red, green, and blue and bands.

The GCC vegetation index was chosen as it is widely used in the Arctic to monitor vegetation greenness (e.g., Anderson et al. 2016, Westergaard-Nielsen 2017, Parmentier et al. 2021), and produces simple frequency curves appropriate for senescence modelling.

Green-Red Vegetation Index (GRVI) values were also calculated using the extracted RGB data but were not used for analysis as they produced complex curves (akin to polynomials of the 4th degree) that complicated senescence modelling. Extracted RGB data remains available for further vegetation index calculation.

3.4.1.3 Senescence modelling

To assess the development of the growing season and the onset of senescence across all AOIs and plots a simple 'spectral senescence model' was devised. It consisted of the following steps:

1) The maximum GCC/NDVI value for each AOI/plot was identified and labelled as 100% greenness. From this maximum value, values of 75%, 50% and 25% greenness were calculated.
2) A line graph with loess smoothing, span = 0.6, was plotted for each AOI/plot using the 'ggplot2' package (v. 3.4.2, Wickham et al., 2023).
3) Intercept lines were drawn over the graphs at the previously identified 75%, 50% and 25% GCC/HDVI values, estimating the following senescence-related DOYs:
    - right side 75% = beginning of senescence DOY (bos_doy),
    - right side 50% = full senescence DOY (fs_doy), and
    - right side 25% = max senescence DOY (ms_doy).

    The packages 'reshape' (v. 0.8.9, Wickham, 2022) and 'tidyr' (v. 1.3.0, Wickham et al., 2023) were used during this step.

4) From the identified DOYs senescence length was calculated:
    - sen_length = ms_doy MINUS bos_doy.

As landscape camera data for the entire growing season was available, the DOYS for left side 25% = active snowmelt DOY (as_doy), left side 50% = beginning of greening DOY (bog_doy), left side 75% = full greening DOY (fg_doy), as well as median peak DOY=

(fg_doy PLUSS bos_doy)/2, greenup length in days (gu_length = mp_doy MINUS bog_doy), full greening in days (fg_length = bos_doy MINUS fg_doy), and growing season in days (gr_season = bos_doy MINUS bog_doy) were also estimated, and are available for further growing season analysis. To answer questions about the length of the growing season in snow accumulated plots, as_doy and gr_season were used. The spectral model is here illustrated in figures 3.11a-c:

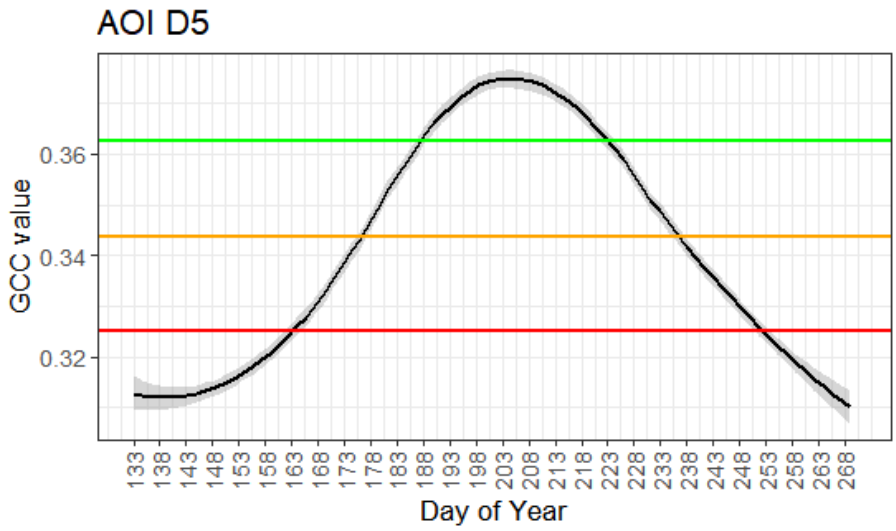

Figure 3.11a: GCC spectral model curve with intercepts, here illustrated by AOI D5. Topmost intercept = 75% GCC, middle = 50% GCC, lower = 25% GCC.

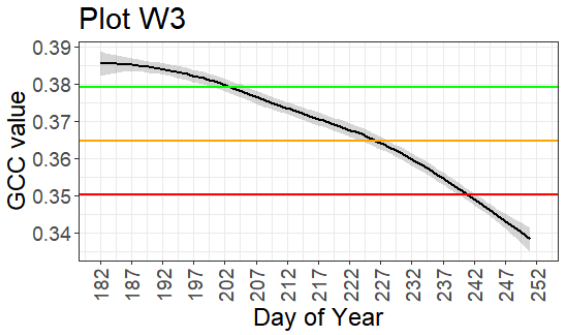

Figure 3.11b: GCC spectral model curve with intercepts, here illustrated by plot W3. Topmost intercept = 75% GCC, middle = 50% GCC, lower = 25% GCC.

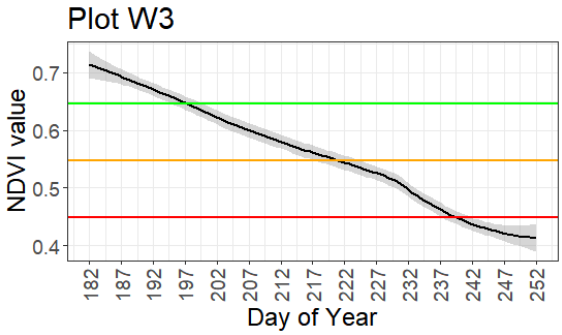

Figure 3.11c: NDVI spectral model curve with intercepts, here illustrated by plot W3. Topmost intercept = 75% GCC, middle = 50% GCC, lower = 25% NDVI.

Divergence and removal

During RGB extraction and spectral senescence modelling one of the plots (C2) and one AOI (E7) displayed divergent greenness/senescence patterns against the norm and were excluded from the analysis. The C2 camera was at fault for the exclusion of the C2 plot, as the images it produced were of a different quality from the other cameras, and thus registered differently in the GCC vegetation index. For the landscape camera, E7 most likely had a greater water content presence than initially assumed during AOI mapping, off-setting the greenness values from the vegetation present. Curves for both C2 and E7 can be found in the Appendix, figures A3.3 and A3.4.

3.4.2 Exploratory variables

Like image data, all exploratory sensor measurements used in plot analysis were taken between DOY 182 (July 1st, 2022) and DOY 256 (September 13th, 2022).

3.4.2.1 NDVI

Daily NDVI means were calculated using all 12 measurements throughout polar day and then using 6 of the 12 measurements starting from the first sunset of the season, on DOY 235 (August 23rd, 2022). Measurements used post-sunset were taken between 8 am and 6 pm, to control for blue band interference as far as possible.

None of the plots had any missing NDVI values. However, the NDVI values for plots C2, C3 and N3 had to be calculated, as the sensors only registered the red and infrared bands, without doing the calculation the other sensors did. The supplied formula from the sensor handbook was used, figure 3.12:

$$NDVI = \alpha Rn - Rr / \alpha Rn + Rr$$

Figure 3.12: NDVI calculation formula from sensor handbook. α = Ir/In = 1,4. Rn = the reflected NIR radiation from the canopy = 810. Rr = the reflected red radiation = 650.

Using the spectral senescence model, the following DOYs were estimated for the plots:

- right side 75% = beginning of senescence DOY (bos_doy),
- right side 50% = full senescence DOY (fs_doy), and
- right side 25% = max senescence DOY (ms_doy).

Senescence length was then calculated (sen_length = ms_doy MINUS bos_doy).

3.4.2.2 Soil moisture

Daily averages for soil moisture were calculated using the available data from between DOY 182 and DOY 256. The N1 sensor had a few missing values towards the end of the season starting from August 25th, where means were calculated from the available data. Due to equipment malfunction no measurements were available for plot N3.

3.4.2.3 Soil temperature

Daily averages for soil temperature were calculated using the available data from between DOY 182 and DOY 256. Due to equipment malfunction no measurements were available for plot N3.

3.4.2.4 Soil samples

Soil samples were analysed for nitrogen and loss on ignition (LOI) content through a method of near-infrared spectroscopy (NIRS) developed at UiT for leaf and soil nutrient content prediction. Analysis models for soil nutrient content were calibrated using samples from Finnmark and Svalbard, comparing NIRS analysis results to results from standard chemical nutrient content analyses (Murguzur et al., 2019).

Soil samples from the plots were dried at 60°C for 48 hours, before being placed in a small petri dish and scanned 5 times each by a Maglite connected to a Field spec 3. The petri dishes were rotated with each scan, and a new baseline was taken with a white reference spectralon every 30 minutes. The resulting .asd files were converted using the aforementioned models in R, means were calculated and entered into a data set.

As no other nutrient analysis was done of the soil samples, NIRS results are to be interpreted as estimates.

3.4.2.5 Leaf length

Due to great variance in size between Site #2 and the others, leaf length means were log10-transformed for analysis. Where sites #1 and #3 had mean untransformed leaf length of approximately 8 mm, leaves at Site #2 were on average 8-9 cm in length. Due to great physiological similarity, leaves of *Dupontia fisheri* and *Eriophorum scheuchzeri* were not differentiated during the measurement process. Bryophytes at Site #2 were not measured, neither was a *Saxifraga oppositifolia* plant present in plot W1.

3.4.3 Statistical analysis

3.4.3.1 Data cleaning

Data was cleaned on a group level, (GCC, NDVI, etc) to remove obvious erroneous outliers and noise, to either its 99^{th} (plots) or 95^{th} (landscape camera) percentile.

3.4.3.2 Regional regrouping

To keep the groups of a similar size for testing and comparison, region A was split into two 'subregions': region AA (AOIs A1-A12) and region AB (AOIs A13-A21).

3.4.3.3 Sample size – nutrient analysis

With the loss of the C2 plot, the sample size for the experimental plots was reduced to 8 samples. This is a very small sample size, which is often insufficient for a robust mixed linear analysis. Smaller sample sizes may result in reduced statistical power, making it more challenging to detect meaningful effects or accurately estimate parameters. Additionally, smaller sample sizes may cause increased variability and less precision in estimates, potentially compromising the generalisability and reliability of the findings. Power assessments for a t-test and linear regression with a sample size of 8, an effect size of 0.8, and significance level 0.05 produced values of 0.232 and 0.208 (1000 simulations). With low test power, the chance for Type II error (false negative) is higher, as small sample sizes often lack sufficient statistical power to detect meaningful relationships. With limited data, it becomes challenging to distinguish between random fluctuations and true effects, which again can lead to inconclusive or misleading results.

Analytical power was further reduced by the fact that the missing variable was a control plot, which effectively removed the Site #2 baseline from the dataset. As Site #2 had a different vegetation, moisture, and soil profile than the other two, control plot inference from Sites #1 and #3 would be less reliable than if the missing control plot came from one of the other sites, which had more similar profiles. The DOY for beginning of senescence was also missing from the dataset for the nutrient plot of Site #2.

To offset these issues, analysis of plot data was kept as simple as possible, with results serving as indicators more so than answers.

3.4.3.4 Testing and modelling

Statistical analysis was done in RStudio (v. 421, Posit, PBC, 2023), using R (v. 4.2.3, R Core Team, 2023). Anova and AICc ('AICcmodavg', v. 2.3-2, Mazerolle 2023) were used to assess variable relationships and aid in model selection.

Several tests were done to assess difference between condition groups in the landscape camera data. Due to the unequal number of ambient and green AOIs, the non-parametric Mann-Whitney U test was applied on a regional level. The whole data set was tested with both a Mann-Whitney U test, as well as a Tukey HSD test as there were more AOIs in both groups. Additionally, One-sample t-test was done against a set mean for ambient AOIs for the regions that had normally distributed green AOI data. To investigate the relationship between snow melt and growing season length, a simple linear model was devised: *lm(gr_season_gc ~ as_doy_gcc)*. The relationship between snowmelt and maximum greenness (100% GCC) was assessed through the linear model: *lm(gcc_100 ~ as_doy_gcc)*. AICc identified the best linear model for onset of senescence for the landscape camera data to be *lm(bos_doy_gcc ~ condition + region)*, explaining 25% of the variation in the data. AICc table in appendix, T3.1.

Differences between treatments groups for the plots were assessed with a pairwise t-test overall, and for all sites. Simple linear models (1 predictor) were used to assess relationships for the plot data.

4 Results

4.1 Onset of senescence

4.1.1 Maximum greenness – landscape camera

Figure 4.1 shows the maximum greenness (GCC 100%) as measured by the spectral model for image data from the landscape camera. It was significantly greater for green AOIs than for ambient ones overall ($p << 0.01$), as well as throughout the regions AA + B-E ($p < 0.01$), with the exception of region AB. Additionally, region D distinguished itself as significantly greener than the other regions overall ($p \leq 0.02$), as seen in figure 4.2.

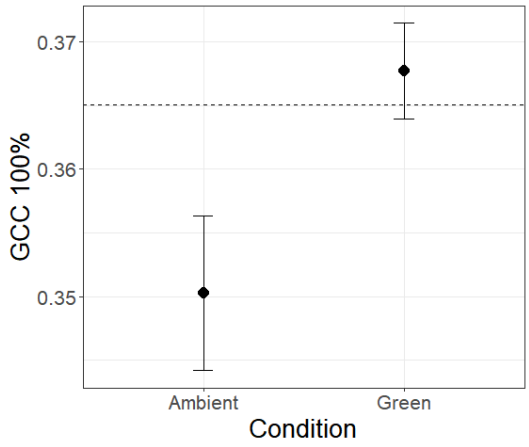

Figure 4.1: Maximum greenness level (GCC 100%) means and with their 95% confidence intervals for the two conditions, ambient and green. Dashed line marks the overall mean of the data.

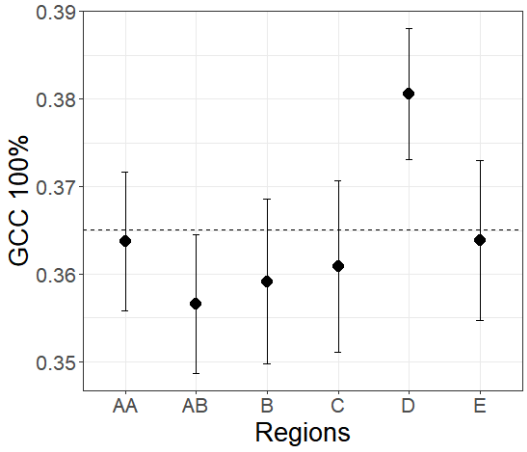

Figure 4.2: Maximum greenness level (GCC 100%) means and their 95% confidence intervals for all five regions, both conditions. Dashed line marks the overall mean of the data.

Boxplot displaying the data distribution and means of each condition for each region can be found in the Appendix, figure A4.1.

A linear model with GCC 100% as a predictor variable showed a $p << 0.01$ against response variable beginning of senescence DOY. As these are related variables, the positive relationship between them suggests the existence of (a) confounding variable(s) affecting both greenness levels and senescence onset for AOIs. Model output can be found in the Appendix, table T4.1.

4.1.2 Senescence onset

The difference between the beginning of senescence estimated by the spectral model for the green and ambient AOIs was found to be slightly significant (One-sample t-test: $p = 0.0543$, Mann-Whitney U test: $p < 0.05$), as illustrated by figure 4.4.

Regions D displayed a significant delay for the beginning of senescence compared to region AA ($p < 0.02$) and B ($p > 0.01$) for both conditions combined, illustrated by figure 4.5.

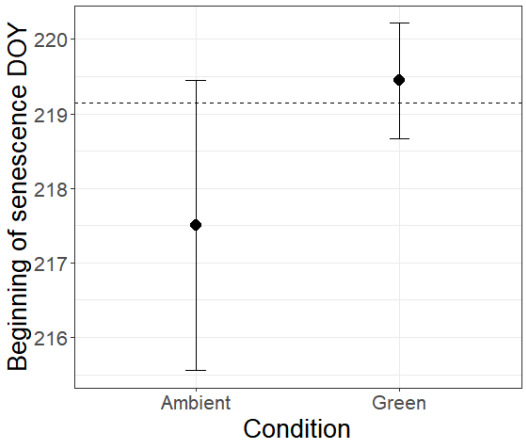

Figure 4.4: Beginning of senescence DOY means and their 95% confidence intervals for the two conditions, ambient and green. Dashed line marks the overall mean of the data.

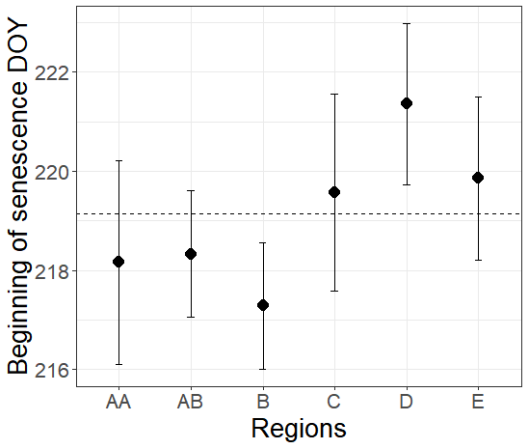

Figure 4.5: Beginning of senescence DOY means and their 95% confidence intervals for all five regions, both conditions. Dashed line marks the overall mean of the data.

Significant difference in means between conditions was found for the regions AB ($p = 0.01$) and D ($p < 0.01$).

The best fit linear model (Beginning of senescence DOY ~ Condition + Region) supported these results, as did a single-predictor linear model for conditions. (Appendix, Tables T3.1 and T4.2). NDIV showed no significant relationship here.

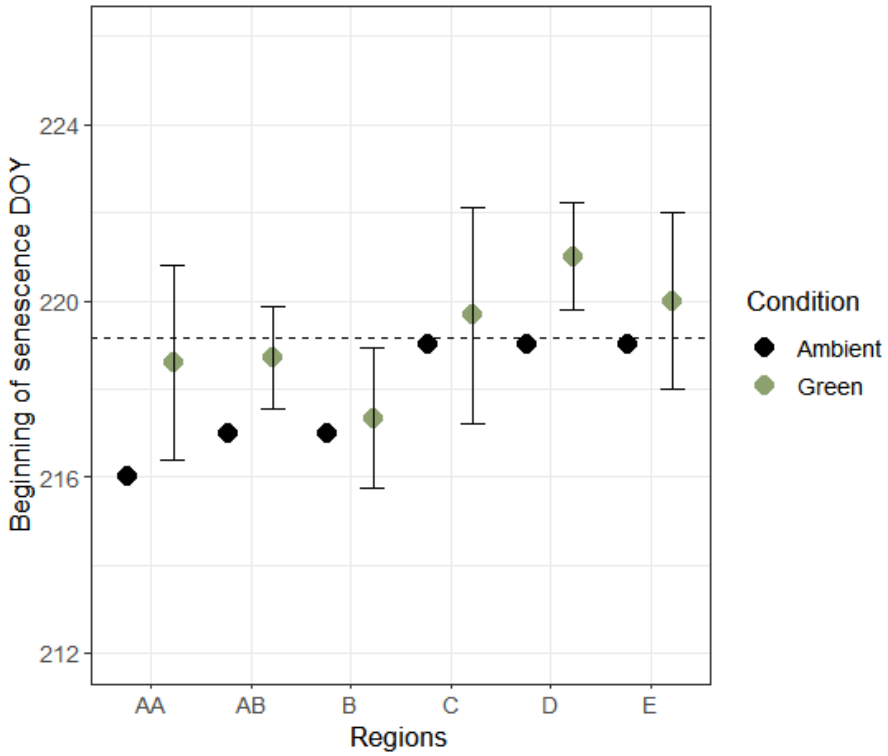

Figure 4.6: Beginning of senescence DOY means, with 95% confidence intervals, for green areas. Central dots indicate condition mean by region, while the dashed line marks the overall mean of the data.

4.1.2.1 Full senescence, max senescence, and senescence length

Three other senescence variables were tested for significance between conditions: Full senescence DOY (GCC 75%), max senescence DOY (GCC 25%), and senescence length (in days). None were positive for total difference between conditions. Green areas reached full senescence DOY on average after ambient ones but showed no significant difference on a regional level.

Due to noise toward the end of the growing season, six AOIs did not have max senescence values. Three of the AOIs were from region E, two from region A and one from region D. Half (A4, D10, E4) were green condition AOIs, while the other has were ambient AOIs (A17, E2, E8).

Max senescence DOY showed no unified trend. Region E lacked the values for both ambient AOIs and was removed from the analysis. Regionally, significant differences between max senescence DOY were found in region AA only ($p << 0.01$), with ambient AOIs reaching

senescence later than green AOIs. This was also the case, although non-significantly, for region C. Region D had one green outlier reaching max senescence later than the ambient mean.

Boxplots displaying the data distribution and means for full and max senescence DOYs can be found in the Appendix, figures A4.2-3, and A4.4 for senescence length.

Senescence length was greater for ambient AOIs but did not differ significantly for green ones ($p = 0.16$). Region C had the shortest mean senescence length for both conditions but differed significantly only from region AA ($p < 0.02$). Senescence length showed no unified trend between regions, as seen in figure 4.9. In region B ambient areas has shorter senescence on average than green, region AB has little difference between conditions, while in regions AA, C and D green areas had shorter mean senescence length than ambient areas. The following regions showed significant differences in senescence length between conditions: AA ($p < 0.05$) and D ($p << 0.01$). Region E was once again excluded from the analysis due to missing values.

4.1.2.2 Estimated senescence DOYs and senescence length (days)

Table 4.1 shows estimated DOYs for beginning of senescence, as well as full senescence, and max senescence plus senescence length with standard deviation, as identified by the spectral model for data from the landscape camera.

Difference in beginning of senescence between ambient and green plots was two days for the regions AA, D and E. Regions AB and E had a one-day difference, and regions B and C had no difference.

Full senescence began pone day later in green than ambient AOIs in regions AA and B, had no difference in regions AB, C and D, and one day earlier in region E.

Max senescence DOY has great variance between regions. Region AA's green plots reached max senescence ten days earlier than the ambient plots did. For region D it was eight days earlier for green plot, and for C it was two days. For AB and B however, ambient AOIs reached max senescecnce later than green ones, by two days. Region E only had data for green AOIs, so no comparison was here possible.

Table 4.1a-c: Mean days of year for beginning of senescence (Bos DOY), full senescence (Fs DOY) and max senescence (Ms DOY), plus senescence length (Sen length) in days for each region, AA-E, both conditions. DOYS have been rounded to their integers. Standard error (SE) in grey. Mann-Whitney U test (MVU) and One-sample t-test (t-test) results in italic, significant estimates bolded.

a)

	Region AA							Region AB						
					MVU		*t-test*					*MVU*		*t-test*
	Ambient	SE A	**Green**	SE G	*p*	*W*	*p*	**Ambient**	SE A	**Green**	SE G	p	W	p
Bos DOY	216	3,00	218	0,98	*0,382*	*5,5*	-	217	2,00	218	0,47	*0,355*	*3,5*	***0,01***
Fs DOY	233	2,50	234	1,68	*1,0*	*10,0*	0,73	232	3,50	232	0,55	*1,0*	*7,0*	-
Ms DOY	262	0,50	252	1,28	***0,044***	*18,0*	***<< 0,01***	248	-	251	1,60	*0,371*	*1,0*	*0,059*
Sen length	46,5	2,50	34,2	1,27	***0,041***	*18,0*	-	33	-	33	1,46	*0,825*	*4,5*	*1,0*

b)

	Region B							Region C						
					MVU		*t-test*					*MVU*		*t-test*
	Ambient	SE A	**Green**	SE G	*p*	*W*	*p*	**Ambient**	SE A	**Green**	SE G	*p*	*W*	*p*
Bos DOY	217	-	217	0,61	*1,0*	*2,5*	-	219	-	219	0,95	*1,0*	*2,5*	-
Fs DOY	231	-	232	1,52	*1,0*	*2,5*	-	231	-	231	0,83	*1,0*	*2,5*	-
Ms DOY	250	-	252	2,29	*1,0*	*2,5*	*0,39*	250	-	248	0,73	*0,427*	*5,0*	-
Sen length	33	-	34,8	2,40	*1,0*	*3,5*	-	31	-	28,3	0,95	*0,432*	*5,0*	-

c)

	Region D							Region E						
					MVU		*t-test*					*MVU*		*t-test*
	Ambient	SE A	**Green**	SE G	p	W	p	**Ambient**	SE A	**Green**	SE G	*p*	*W*	*p*
Bos DOY	219	-	221	0,76	*0,190*	*0,5*	***< 0,01***	219	0,00	220	0,77	*0,387*	*3,0*	-
Fs DOY	236	-	236	1,19	*1,0*	*5,0*	*0,807*	237	1,00	236	1,35	*1,0*	*6,0*	-
Ms DOY	262	-	254	1,69	*0,287*	*8,0*	-	-	-	260	1,47	-	-	-
Sen length	43	-	32,8	1,22	*0,161*	*9,0*	***<< 0,01***	-	-	40,6	1,29	-	-	-

Senescence length was longer for ambient than green AOIs for all regions except region AB (same length), and E (no data). It was 12.3 days longer for region AA, 10.2 days longer for region D, 2.7 days longer for region C, equal for region AB, and 1.8 days shorter for region B. Region E, once again, lacked the data.

4.1.3 Maximum greenness – plots

The maximum greenness had no significant difference between treatments neither for GCC nor NDVI overall but showed significant difference between sites (GCC $p < 0.03$, NDVI $p < 0.01$). The difference for GCC was found between *Salix* and *Dryas*, with *Dryas* being

significantly greener than *Salix*, and with graminoids placed in the middle. NDVI showed no significant difference in greenness between sites.

As for the plots themselves, GCC and NDVI recorded their maximum greenness in different order, as seen in table 4.2. There was however consensus that the greenest plots were from Site #1 and #2, with Site #3 being the least green.

A linear model with GCC 100% as a predictor variable showed a $p = 0.02$ against response variable beginning of senescence DOY (Appendix, table T4.3). The positive relationship between them once again suggests the existence of (a) confounding variable(s) affecting both greenness levels and senescence onset. A slightly positive relationship between 100% NDVI and beginning of senescence DOY was found, but nothing significant.

Table 4.2: Max greenness values (GCC/NDVI 100%) for all plots, in descending order.

Plot	GCC value	Plot	NDVI value
N1	0,430	N2	0,814
C1	0,415	N1	0,782
W2	0,408	W1	0,753
W1	0,406	C1	0,746
N2	0,404	W3	0,743
W3	0,394	W2	0,725
N3	0,389	N3	0,721
C3	0,379	C3	0,716
C2	-	C2	0,705

4.1.4 Snow melt, greenness, and senescence length

The linear model assessing time of snowmelt and senescence length showed a strong, significantly negative relationship between active snowmelt DOY (25% GCC), and growing season length ($p << 0.01$). This means that as active snowmelt DOY increases, ergo the snow melt happens later in the season, the growing season decreases. The linear model analysis of maximum greenness and active snowmelt DOY showed a significantly positive, but weak relationship ($p << 0.01$). The model outputs can be found in the Appendix, table T4.4A+B.

4.2 Effect of nutrients and water

4.2.1.1 Senescence onset

No significant effect on the onset of senescence (beginning of senescence DOY), neither positive nor negative, was found for any of the treatments. Neither GCC nor NDVI had significant differences between groups (figures 4.10a+b). NDVI showed slightly delayed senescence for nutrient plots, as was not the case for GCC. Water plots look to have senesced somewhat later than the other treatment plots, but with such small sample size and such large confidence intervals interpretation quickly becomes speculation.

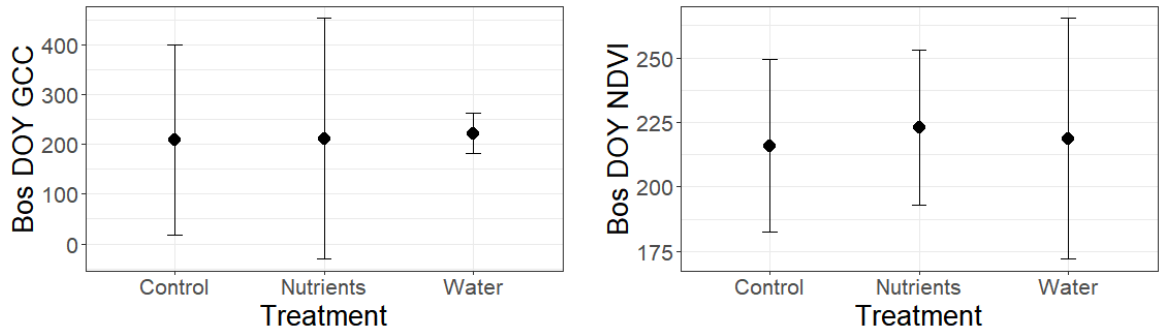

Figure 4.10a-b: Estimated mean beginning of senescence with 95% confidence interval for all treatments, for GCC and NDVI models. Note very large confidence intervals for the GCC model – this due to a reduced sample size.

Significant difference was found in onset of senescence between sites, with Site #1's *Dryas* senescing later than Site #3's *Salix* (GCC $p << 0.01$, NDVI $p < 0.01$). The *Salix* water plot,

W3, also senesced 10 days later than the control and nutrient plots at the same site (table 4.3). The NDVI model showed significantly later average onset of senescence for graminoids at Site #2 than for *Salix* ($p > 0.01$).

Linear modelling using GCC and NDVI values further confirmed significant difference in senescence onset between *Dryas* and *Salix* sites. However, the absence of GCC control and nutrient plots at Site #2, may have affected the GCC model (Appendix, table T4.5A+B).

4.2.1.2 Full senescence, max senescence, and senescence length

Full senescence DOY showed no significance in differences between neither treatments nor sites for GCC. For NDVI there was significant difference in DOYs for sites between *Salix* and *Dryas* ($p < 0.5$) and *Salix* and graminoids ($p < 0.01$), with Site #2's graminoids reaching full senescence later than both of the others. Max senescence DOY showed no significance in difference between treatments or sites neither GCC nor NDVI.

Senescence length was significantly longer at the *Salix* site than at the *Dryas* site for GCC ($p < 0.01$). For NDVI, both *Dryas* and graminoids had significantly shorter senescence than *Salix* ($p < 0.05$ and $p < 0.02$).

Table 4.3a+b: Days of year for beginning of senescence (Bos DOY), full senescence (Fs DOY) and max senescence (Ms DOY), plus senescence length (Sen length) in days for each site, #1-3, all three treatments – GCC and NDVI. DOYS have been rounded to their integers. Note – these are estimates, not means.

a)

	Site 1 - *Dryas*			Site 2 - Graminoids			Site 3 - *Salix*		
	Control	Water	Nutrients	Control	Water	Nutrients	Control	Water	Nutrients
Bos DOY GCC	224	230	230	-	233	-	194	203	192
Fs DOY GCC	232	237	237	-	241	231	222	227	233
Ms DOY GCC	240	244	244	-	249	244	233	241	242
Sen length GCC	16	14	14	-	16	-	39	38	50

b)

	Site 1 - *Dryas*			Site 2 - Graminoids			Site 3 - *Salix*		
	Control	Water	Nutrients	Control	Water	Nutrients	Control	Water	Nutrients
Bos DOY NDVI	212	229	229	231	230	231	205	197	209
Fs DOY NDVI	226	239	237	238	239	239	222	221	224
Ms DOY NDVI	235	248	245	246	249	245	234	239	238
Sen length NDVI	23	19	16	15	19	14	29	42	29

The DOYs for beginning, full and max senescence for the plots can be found in Table 4.3, along with senescence length.

Table 4.4: Senescence length (in days) GCC and NDVI for all plots, sorted in descending order.

Plot	Sen length GCC	Plot	Sen length NDVI
N3	50	W3	42
C3	39	C3	29
W3	38	N3	29
C1	16	C1	23
W2	16	W1	19
W1	14	W2	19
N1	14	N1	16
C2	-	C2	15
N2	-	N2	14

Table 4.4 shows that there was agreement between GCC and NDVI that Site #3 had the longest estimated senescence length compared to sites #1 and #2.

4.2.1.3 Linear relationships

Linear modelling did not reveal any significant relationships between the onset of senescence and the other nutrient-related exploratory variables collected in the field (N and LOI).

Full senescence DOY GCC had a significantly positive relationship with soil nitrogen difference between soil samples taken at the start and end of the field work ($p < 0.05$). A slightly significant positive relationship was found with LOI nutrient content ($p = 0.0521$). Tables in Appendix, T4.6+7.

Max senescence DOY GCC and NDVI displayed a statistically significant negative relationship with peak soil temperature and mean soil temperature ($p < 0.05$, Appendix, T4.8A-D). GCC also had a statistically significant positive relationship with difference in soil nitrogen ($p = 0.01$) and difference in LOI ($p = 0.02$). Tables in Appendix, T4.9+10.

For senescence length, the GCC model had a significant negative relationship with the maximum greenness value GCC 100% ($p = 0.02$, Appendix T4.11).

Tables for all linear relationships are presented in full, to display the information available for the tiny sample size. Only significant and slightly significant relationships are addressed here.

4.3 Exploratory variables

4.3.1 Soil moisture

Site #1 and Site #2 displayed a similar soil moisture curve for the growing season, with first valleys around DOY 225, and second valley just before DOY 250. Site #2 shared the first valley around DOY 225, but increased steeply following that and did not sink again throughout the experiment.

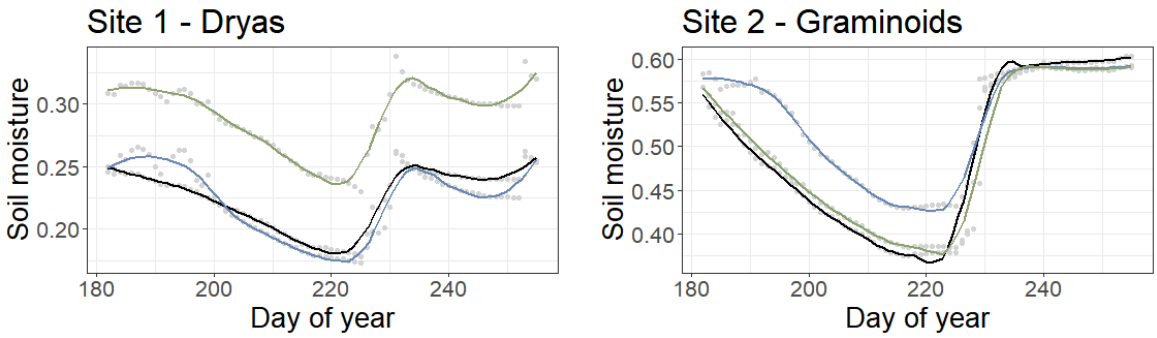

Figure 4.11a-b: Soil moisture (VWC m^3/m^3) for Site 1 and 2. Black = control plot, blue = water plot, green = nutrients plot. Note different moisture scales for each site.

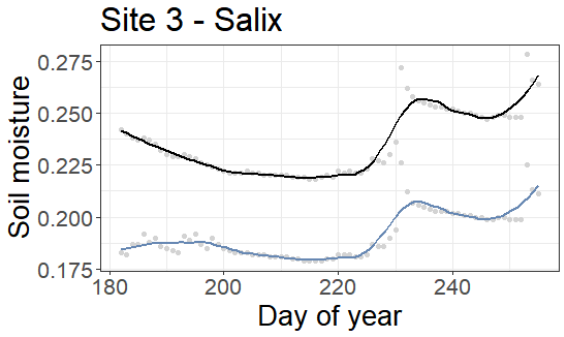

Figure 4.11c: Soil moisture (VWC m^3/m^3) for Site 3. Black = control plot, blue = water plot. Soil moisture data for the nutrients plot at site 3 was missing.

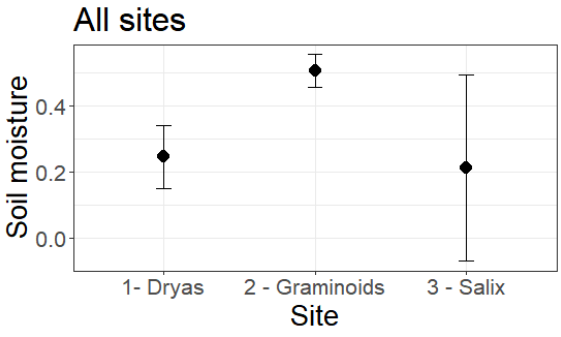

Figure 4.11d: Soil moisture (VWC m^3/m^3) means with their 95% confidence intervals for all sites.

Water addition to treated plots does not seem to have had any lasting effect on the soil moisture profile at the sites, as seen in figure 4.11a-c. It is difficult, however, to assess whether the additional water made a difference in soil moisture content at water and nutrient

plots. Treatments were added to the plots up until just approximately DOY 200, which can be seen in a slight peak for the water and nutrient plots of Site #1, and the water plots of Site #2 and #3. The nutrient plot at Site #2 does not seem to have been affected. The decrease in soil moisture returned to displaying the same patterns as the control sites once treatments stopped. The only plot where water content remained high through the DOY 200 valley was plot W2, However, as with the other plots, this difference may stem from preexisting plot conditions.

The soil was however significantly wetter at site 2 than the site 1 and 3 ($p << 0.01$ – figure 4.11d).

4.3.2 Soil temperature

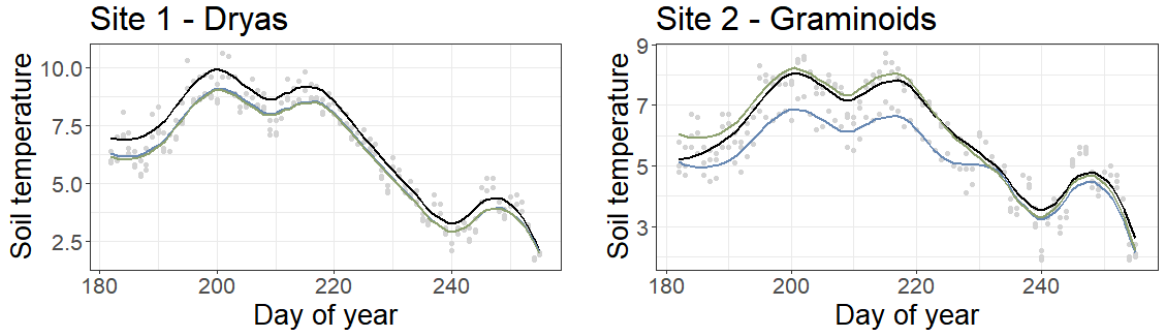

Figure 4.12a+b: Soil temperature (°C) for Site 1 and 2. Black = control plot, blue = water plot, green = nutrients plot. Note slightly different temperature scales for each site.

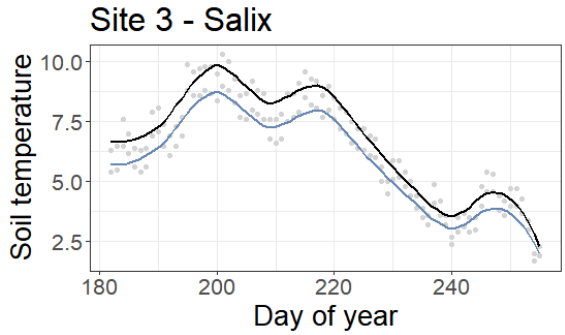

Figure 4.12c: Soil temperature (°C) for Site 3. Black = control plot, blue = water plot. Soil temperature data for the nutrients plot at site 3 was missing.

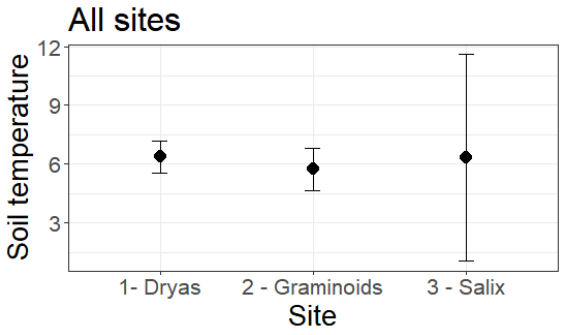

Figure 4.12d: Soil temperature (°C) means with their 95% confidence intervals for all sites.

Soil temperature was not significantly different between sites (figure 4.12d). All three sites displayed a temperature pattern with two peaks around DOY 200 and 215, with a valley at around DOY 240, as can be seen in figures 4.12a-c. No treatment-related temperature pattern was observed in the data.

4.3.3 Soil nutrients

Difference in soil nutrients estimates between start and end of the fieldwork showed no significant differences between neither sites nor treatments for neither N nor LOI. N and LOI taken at the beginning of fieldwork had no significant difference between plots or treatments. Values from the end of fieldwork showed significant differences between treatments for both N and LOI (figures 4.13a-b).

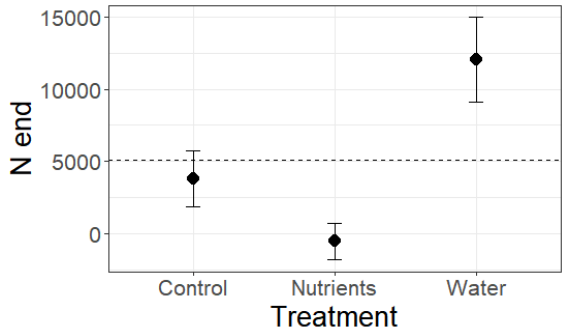

Figure 4.13a: Difference in estimated N-content at the end of field work for each treatment. Significant difference between all treatments ($p << 0.01$). Dashed line marks the overall mean of the data.

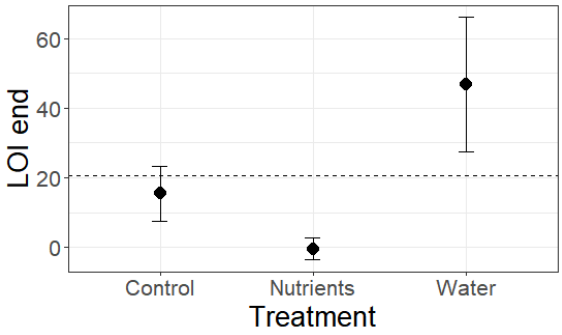

Figure 4.13b: Difference in estimated LOI-content at the end of field work for each treatment. Significant difference between all treatments ($p < 0.03$ for nutrients and control, water's relationships $p << 0.01$). Dashed line marks the overall mean of the data.

4.3.4 Leaf length

Log-transformed leaf length means showed no significant difference between treatments for any of the samples. Between sites, graminoids were significantly different form both *Dryas* and *Salix* ($p << 0.01$ - figure 4.14a).

At a site-level, Site 2 had no significant difference between treatments. At Site #1 control plot leaves were significantly longer than nutrient plot leaves ($p << 0.01$). At Site 3, nutrient plot leaves were significantly longer than both control and water ($p << 0.01$). See figure 4.14b-d.

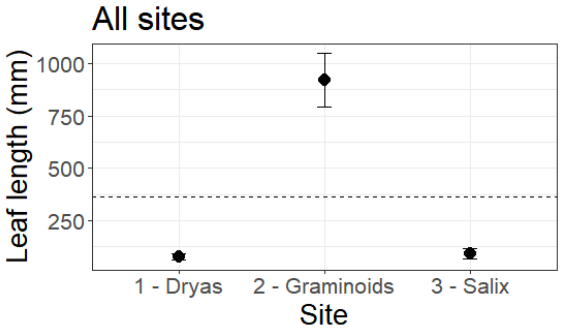

Figure 4.14a: Difference between leaf length means with their 95% confidence intervals for the sites. Dashed line marks the overall mean of the data.

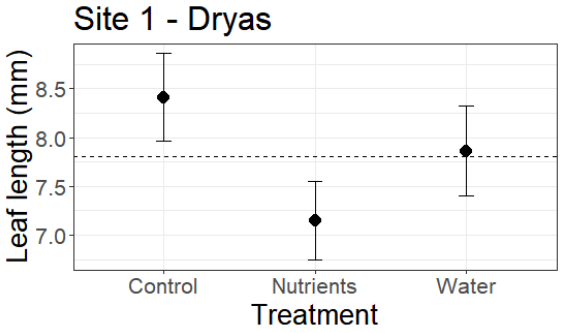

Figure 4.14b: Difference between mean leaf length with 95% confidence interval for all treatments, Site #1. Dashed line marks the overall mean of the data.

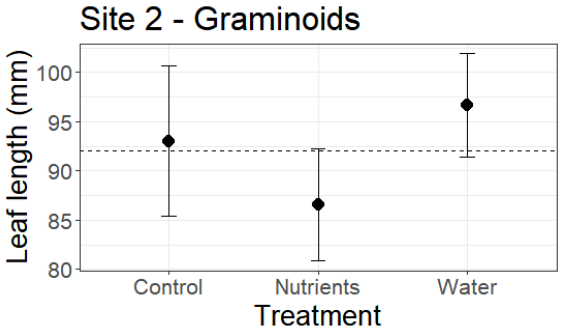

Figure 4.14c: Difference between mean leaf length with 95% confidence interval for all treatments, Site #2. Dashed line marks the overall mean of the data.

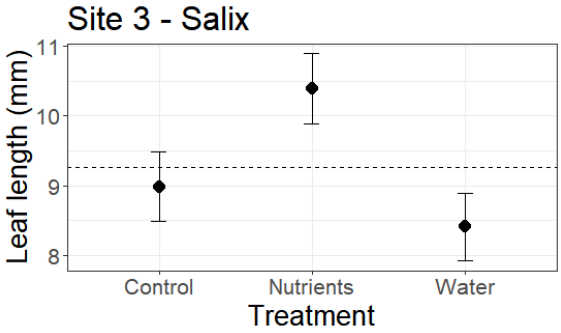

Figure 4.14d: – Difference between mean leaf length with 95% confidence interval for all treatments, Site #3. Dashed line marks the overall mean of the data.

4.3.5 Image comparison – GCC and NDVI

Visual assessment of images estimating beginning of senescence, full senescence, and max senescence for both GCC and NDVI display a greenness decrease/redness increase gradient.

As shown in table 4.3, senescence starts, progresses, and lasts differently for the GCC and NDVI model. For plot N3, senescence is the longest in the GCC-model, 50 days, and shorter in the NDVI model, 29 days. The process is more subtle in the NDIV-estimated images, while being more clearly green, yellow, and red in the GCC-estimated images. Leaf loss and presence of dead plant material is likewise more obvious in the GCC images. Displayed side by side in comparison (figure 4.15), the GCC model looks to be the superior estimator for end of season phenological changes for plot N3. However, a proper, thorough analysis of model performance against on-site observations is necessary to draw further conclusions.

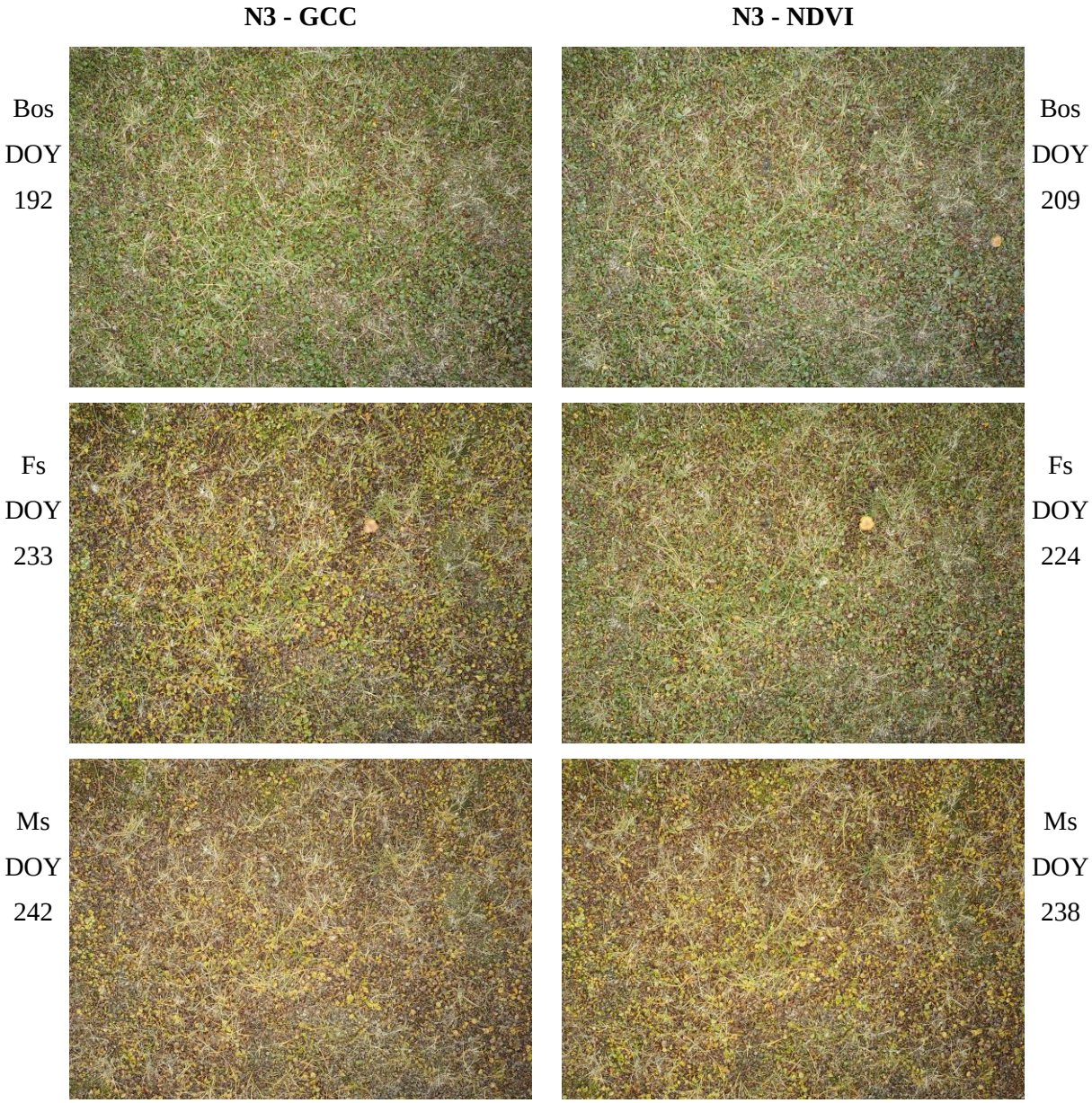

Figure 4.15: Bos, Fs and Ms DOYs, as estimated by the GCC and NDVI models for plot N3 – nutrient addition at the *Salix* site. The DOYs are, in ascending order, July 11, July 28, August 12, August 21, August 26 and August 30, 2019.

5 Discussion

5.1 Summary of results

5.1.1 Delayed senescence onset

Results estimated from the spectral senescence model show that greener areas senesce later than ambient areas, albeit only slightly significantly. The mean of the green areas lies just within the confidence interval of the ambient areas – the size of which is affected by the small number of ambient AOIs in comparison to green ones. Study design may have created the discrepancy between t-test and linear model results of slight significance and the significant Mann-Whitney U result. A repeat of landscape image analysis with a different study design, e. g. one that splits the ambient areas into more samples may help further clarifying the issue.

An agreed upon p value of < 0.06 remains a decent indicator of a strong, positive relationship between high levels of greenness output, as estimated by the spectral senescence model, and delay in onset of senescence – further supported by the strong, significantly positive linear relationship between GCC 100% and beginning of senescence for both AOIs and plots.

Areas that experienced later snowmelt as defined by the variable active snowmelt DOY, experienced a significantly shortened growing season as estimated by the spectral model. A positive and significant, but weak, relationship was found between maximum greenness and active snowmelt DOY for the landscape camera data.

5.1.1.1 Senescence development and length

What differences there were for full senescence and max senescence, took place on a regional level for the landscape camera data. Full senescence started on average later for green AOIs, but the difference was non-significant. Plot data, albeit limited by a small sample size, displayed a significant delay in greendown between sites, as measured by NDVI, and more specifically plant groups: the dwarf shrubs at Site #1 and #3 reached full senescence sooner than the graminoids at Site #2. GCC data displayed no clear full senescence trends. Max senescence displayed no uniform pattern for neither data set, either. For the landscape camera max senescence varied greatly, with 3/5 analysed regions showing an opposite trend, with ambient areas coming to max senescence later than green ones. For the plots, no strong trends were found neither for GCC nor NDVI.

A later onset of the beginning of senescence and a similar DOY for max senescecnce for green and ambient AOIs points toward a longer senescence for the ambient AOIs. Which is the major trend in the data. There were however exceptions, on a region level. Site-wise for the plots, senescence did not differ significantly between treatments, but instead between dominant species: the *Salix* site had significantly longer senescence than both *Dryas* (GCC + NDVI) and graminoids (NDVI).

5.1.2 Role of nutrients and water

The role of nutrients in the onset of senescence remains nebulous, especially in lieu of the small sample size of the experiment. No direct positive relationship between the addition of nutrients and delayed senescence onset was found for any of the sites. Significant difference in senescence onset for the plots was not found between treatments, but between sites – and by extension, plant groups. The loss of both the C2 camera data, as well as the absence of Bos DOY values for the nutrient plot at Site #2 affects these results. The remaining plots show divergent patterns: the *Dryas* nutrient plot senesced later than the control plot – but earlier than the water plot. The *Salix* nutrient plot senesced earlier than both control and water.

Senescence development variables, full and max senescence, continue the same lack of overall trend for nutrient-added plots. Only NDVI comparison for full senescence of nutrient plots showed a significant delay between full senescence for graminoids versus *Dryas* and *Salix*. Senescence length was as mentioned significantly longer for *Salix* plots against the two others, *Dryas* in both the GCC and NDVI models, and graminoids in the NDVI model.

Soil nutrient content was found to have a positive, statistically significant relationships with full senescence DOY for the plots (N), and a negative significant relationship with max senescence DOY (N + LOI). Meaning that higher N values in the soil correlated with a delayed full senescence, and with an advanced max senescence. LOI content in the soil had the same relationship as nitrogen, but only significantly for max senescence. At the end of the field work, on DOY 198, all plots showed significantly more N and LOI content in water plots, than in control and nutrient-treated plots, with nutrient plots having the lowest N and LOI values.

In terms of leaf length, the sites once again responded differently. *Dryas* leaves were longest

at the control site. Graminoid leaf length had a slight, negative relationship with nutrient addition, and *Salix* had a strong, significantly positive relationship between leaf length and nutrient addition.

5.2 Senescence in a changing Arctic

Carefully considering the results of the experiment, the effect of increased nutrient availability in High Arctic soil may just be site- and vegetation-type specific. The nutrient response of one species, may thus not translate to another – a pattern which corresponds with the literature (Klokk & Rønning 1987; Gordon et al. 2001; Klanderud 2008). Watering treatments likewise failed to produce any unified response from the studied plant communities.

The *Dryas* plots, that from literature were expected to have an intermediary response to nutrient treatment (Baddeley et al. 1994), showed a consistent DOY-delay in senescence onset and development, and had shorter senescence length than the other plots in both the GCC and NDVI indices. *Salix*, which in earlier studies was most responsive to nutrient addition (Baddeley et al. 1994; Robinson et al. 1998), funnelled the added nutrients into growing bigger leaves. Graminoids displayed the opposite effect: the nutrient plot was the plot with the smallest leaves. This may have been due to the fact that the lower vegetation layer beneath the graminoids was made up of a bryophyte carpet. Bryophytes respond quickly and strongly to nutrient addition (Klokk & Rønning 1987; Neby et al. 2021). The bryophytes may have simply taken the nutrients from the soil more effectively than graminoids could, leaving less than normal nutrient content behind for the graminoids to metabolise. This is however speculation and remains to be tested in the field.

Excessive nutrient addition does not necessarily benefit plants. Plants at lower latitudes experience prolonged sub-optimal environmental conditions as stressors (Bohnert & Sheveleva 1998). Perhaps Arctic plants likewise experience sudden nutrient and water additions as stress and respond adversely. Studies have found negative vegetation response to the addition of nutrients, leading to both physiological damage to plants, as well as reduction in vegetation (Forbes and Jefferies 1999; Gordon et al. 2001; Hussein et al. 2021). At extreme levels, water in the form of flooding has been known to deplete soil oxygen and alter plant metabolism in a way that inhibits growth. The closing of stomata reduces photosynthesis as

well as mineral absorption, carbohydrate translocation and alters plant hormone balance (Kozlowski 1984). The Arctic has historically been a cold, nutrient-limited desert, with dry, poor conditions for growth. Traits that benefit plants that thrive under such conditions may limit their success following the coming climate changes.

Soils were not tested for pH following nutrient and water addition, neither were they tested for increased conductivity, which has been documented in cases of increased potassium (K+) ion concentrations (Zwolicki et al. 2012). Changes in these values may reveal relevant relationships affecting senescence processes. Soil pH has been found to be the key environmental condition structuring Arctic soil biota: specialist taxa were found to be the most abundant in alkaline and acidic soils, while generalist taxa were found to be more abundant in acidoneutral soils (Malard et al. 2019). Sudden changes to the natural state of soil biota communities may bring unexpected. No analysis of soil biota was done to see if nutrient addition affected decomposition, which would be especially relevant at Site #2, where easily decomposable bryophytes were present.

The end of senescence appears more uniform than the beginning, indicating a unifying Adventdalen-wide driver, which points toward abiotic factors such as light and temperature. In 2019, the sun set on DOY 235, August 23rd, 2022. Which correlates roughly with both soil moisture valleys and soil temperature peaks for the plots. The continuous warmth of the sun helps heat soil and evaporate water, so when the sun sets, this dynamic changes. Adventdalen plants have been found to display strong periodicity, which may be an adaptation to the historically short and cold growing season that lacks the light cues of lower latitudes (Semenchuk et al. 2016). However, senescence onset on the High Arctic tundra of Northeast Greenland has been documented to be delayed by 15 days by a warming increase of 2.5°C (Marchand et al. 2004).

Another interesting parameter to look at could be organic soil depth, in terms of microbiota relationships as well as root networks. Plant metabolism and metabolic processes could give insight into how nutrients travel through Arctic plant species and communities. The effect of the amount of dead material in the plots, and plant nitrate reduction levels could also be worth considering.

Thus, senescence in the Arctic remains a complex, multifaceted process, showing no clear overall trends or tendencies in response to changing climatic conditions. Though, again, the sample size for the nutrient experiment was small, and would benefit from repetition.

5.3 NRS standardisation

5.3.1 Modelling senescence

GCC and NDVI showed similar patterns for onset and development of senescence for the plots, a correlation between confirmed by the literature (Richardson et al. 2007; Westergaard-Nielsen et al. 2013). A proper comparison was not done between the two here due to the small sample size of the of the experiment, with its limited power. There were some differences between the index estimates, but both identified differences in senescence onset between sites and treatments, as well as full senescence, max senescence, and senescence length. Preliminary GCC/NDVI comparison for senescence development DOY estimates suggests that GCC may correlate better with end of season observations than NDVI. This remains to be tested on a larger scale. Studies shows that GCC and NDVI do correlate, both in time and space.

Where the NDVI vegetation index uses only red and infrared bands to estimate greenness, the GCC index uses the red, green, and blue. There are therefore bound to be differences between GCC and NDVI estimates. Some vegetation features are easier to assess using NDVI, while others are easier to assess using GCC – or other RGB image-based indices – like areas dominated by graminoids (NDVI), and areas dominated by the bryophyte *Aulacomnium turgidum* (GCC, Tømmervik et al. 2014). Like NDVI (Karlsen et al. 2018), GCC can also be used as a proxy for gross ecosystem productivity and performs well in very low productive Arctic regions (Westergaard-Nielsen et al. 2017).

As both NDVI sensors and GCC are low-cost and low maintenance NRS alternatives, using them together in the High Arctic gives more depth to senescence analysis: All plants are not created equally green. Regions dominated by plants like the predominantly red-brown *Cassiope tetragona* as well as the bright pink/purple-flowered *Saxifraga oppositifolia* that turns largely red-post bloom (illustrated in Lee & Elvebakk, 2019), may obscure actual vegetation richness estimates at a distance – such as the images from the landscape camera. Such plots may therefore get marked as ‘ambient’ due to their lack of greenness, even though

they are productive. Supplied with RBG images at a closer range, from which GCC estimates are to be derived, vegetation may be identified more accurately when in doubt.

GCC spectral senescence development with has previously been modelled both through second degree polynomials and sigmoid curves for (Buus-Hinkler et al. 2006 and Tamstorf et al. 2007, as cited in Westergaard-Nielsen et al. 2017). A simpler to execute loess smoothing model has been found to produce, with the right calibrations, very precise results for NDVI data (Cai et al. 2017). The spectral senescence model presented here has is a first step towards adapting and assessing the loess smoothing approach for GCC data from the High Arctic.

To avoid DOY data loss toward the end of the season (max senescence – and thus senescence length), a different percentage value can be set as the max senescence value instead of 25%. Even for AOIs that did not lose max senescence values, there was a general trend in a higher mean noise-value at the end of the growing season, than at the beginning.

5.3.2 Equipment notes

To capture a full 1 x 1 m plot, and account for camera shaking, camera racks much be taller, somewhere between 1,5 and 2 m.

The *Fricam* camera image output does not correlate very well with the other RGB cameras and does not produce a comparable model curve. Using it to monitor senescence together with Browning Trail Cameras is not recommended.

6 Conclusion

Areas with naturally enhanced moisture and nutrients – identified as ‘green’ areas for the spectral senescecnce model – showed a strong, almost significant delay in onset and development of senescence. Day of year of active snowmelt and maximum GCC greenness value were positively, significantly, but weakly related.

Plots with experimentally enhanced moisture and nutrients showed no unified trend in delay of senescence and responded to nutrient and water addition on a site/vegetation type-level. The plot experiment would however benefit from being repeated, as the sample size was here was very small, and thus not very powerful.

Plant senescence did not happen later for snow accumulated plots. The growing season was instead significantly shortened.

7 References

Anderson H, Nilsen L, Tømmervik H, Karlsen S et al., 2016. Using ordinary digital cameras in place of near-infrared sensors to derive vegetation indices for phenology studies of high arctic vegetation. *Remote Sensing*, 8(10), p. 847. doi:10.3390/rs8100847

Anderson H, Nilsen L, Tømmervik H et al., 2017. Correction: Anderson, H.B. et al. Using ordinary digital cameras in place of near-infrared sensors to derive vegetation indices for phenology studies of high arctic vegetation. Remote Sens. 2016, 8, 847. *Remote Sensing*, 9(10), p. 1003. doi:10.3390/rs9101003

Arens S, Sullivan P & Welker J, 2008. Nonlinear responses to nitrogen and strong interactions with nitrogen and phosphorus additions drastically alter the structure and function of a high arctic ecosystem. *Journal of Geophysical Research*, 113(G3), p. G03S09. doi:10.1029/2007jg000508

Arlov T, 2003. *Svalbards historie*. Trondheim: Tapir Akademisk Forlag.

Baddeley J, Woodin S & Alexander I, 1994. Effects of increased nitrogen and phosphorus availability on the photosynthesis and nutrient relations of three arctic dwarf shrubs from Svalbard. *Functional Ecology*, 8(6), p. 676. doi:10.2307/2390226

Barr S, (2022). Svalbard – Store norske leksikon. [Internet] *Store norske leksikon*. Available from: https://snl.no/Svalbard [Accessed 15.11.2022].

Bigger C & Oechel W, 1982. Nutrient effect on maximum photosynthesis in arctic plants. *Ecography*, 5(2), p. 158-163. doi:10.1111/j.1600-0587.1982.tb01031.x

Bohnert H J & Sheveleva E, 1998. Plant stress adaptations – making metabolism move, *Current Opinion in Plant Biology*, 1(3), p. 267–274. doi:10.1016/s1369-5266(98)80115-5.

Cai Z, Jönsson P, Jin H et al. 2017. Performance of smoothing methods for reconstructing NDVI time-series and estimating vegetation phenology from Modis Data. *Remote Sensing*, 9(12), p. 1271. doi:10.3390/rs9121271.

Cooper E, Dullinger S, Semenchuk P, 2011. Late snowmelt delays plant development and results in lower reproductive success in the High Arctic. *Plant Science*, 180(1), p. 157-167. doi:10.1016/j.plantsci.2010.09.005

Cooper E, 2014. Warmer shorter winters disrupt arctic terrestrial ecosystems. *Annual Review of Ecology, Evolution, and Systematics*, 45(1), p. 271-295. doi:10.1146/annurev-ecolsys-120213-091620

Cooper E, Little C, Pilsbacher A et al., 2019. Disappearing green: Shrubs decline and bryophytes increase with nine years of increased snow accumulation in the High Arctic. *Journal of Vegetation Science*, 30(5), p. 857-867. doi:10.1111/jvs.12793

Elvebakk A, 2005. A vegetation map of Svalbard on the scale 1:3.5 mill. *Phytocoenologia*, 35(4), p. 951-967. doi:10.1127/0340-269x/2005/0035-0951

Engstrom R, Hope A, Kwon H et al., 2008. The Relationship Between Soil Moisture and NDVI Near Barrow, Alaska. *Physical Geography*, 29(1), p. 38-53. doi:10.2747/0272-3646.29.1.38

Forbes B & Jefferies R, 1999. Revegetation of disturbed arctic sites: constraints and applications. *Biological Conservation*, 88(1), p. 15-24. doi:10.1016/s0006-3207(98)00095-0

Fu Y, Piao S, Delpierre N et al., 2019. Nutrient availability alters the correlation between spring leaf-out and autumn leaf senescence dates. *Tree Physiology*, 39(8), p. 1277-1284. doi:10.1093/treephys/tpz041

Gordon C, Wynn J & Woodin S, 2001. Impacts of increased nitrogen supply on high Arctic heath: the importance of bryophytes and phosphorus availability. *New Phytologist*, 149(3), p. 461-471. doi:10.1046/j.1469-8137.2001.00053.x

Hansen A, Herbert R, Mikkelsen K et al., 2007. Viability, diversity and composition of the bacterial community in a high Arctic permafrost soil from Spitsbergen, Northern Norway. *Environmental Microbiology*, 9(11), p. 2870-2884. https://doi.org/10.1111/j.1462-2920.2007.01403.x

Hussein A, Benhamiche-Hanifi S, Baaloudj A et al., 2021. Does seabird colony size determine the physiochemical properties of island soils? *Ekológia (Bratislava)*, 40(3), p. 267-275. doi:10.2478/eko-2021-0029

Karlsen S R, Anderson H B, van der Wal R et al., 2018. A new NDVI measure that overcomes data sparsity in cloud-covered regions predicts annual variation in ground-based estimates of High Arctic plant productivity. *Environmental Research Letters*, 13(2), p. 025011. doi:10.1088/1748-9326/aa9f75.

Klanderud K, 2008. Species-specific responses of an alpine plant community under simulated environmental change. *Journal of Vegetation Science*, 19(3), p. 363-372. doi:10.3170/2008-8-18376

Klokk T & Rønning O, 1987. Revegetation experiments at Ny-Ålesund, Spitsbergen, Svalbard. *Arctic and Alpine Research*, 19(4), p 549. doi:10.2307/1551424

Kozlowski T T, 1984. Plant responses to flooding of Soil. *BioScience*, 34(3), p. 162–167. doi:10.2307/1309751.

Lee Y K & Elvebakk A, 2019, *Handbook of Svalbard Plants*, GEOBOOK Publishing, Seoul.

Lønne I, 2005. Faint traces of high Arctic glaciations: an early Holocene ice-front fluctuation in Bolterdalen, Svalbard. *Boreas*, 34(3), p. 308-323. doi:10.1080/03009480510012971

Lønne I, Nemec W, 2004. High-arctic fan delta recording deglaciation and environment disequilibrium. *Sedimentology*, 51(3), p. 553–589. doi:10.1111/j.1365-3091.2004.00636.x

Malard L A, Muhammad Z A, Carsten S J, 2019. Biogeographical patterns in soil bacterial communities across the Arctic Region. *FEMS Microbiology Ecology*, 95(9), fiz128. doi:10.1101/655431.

Mangerud J, Dokken T, Hebbeln D et al., 1998. Fluctuations in the Svalbard-Barents Sea Ice Sheet during the last 150,000 years. *Quat Sci Rev*, 17(1-3), p. 11-42. doi:10.1016/S0277-3791(97)00069-3

Marchand F, Nijs I, Heuer M et al., 2004. Climate warming postpones senescence in high arctic tundra. *Arctic, Antarctic, and Alpine Research*, 36(4), p. 390-394. doi:10.1657/1523-0430(2004)036[0390:cwpsih]2.0.co;2

Morgner E, Elberling B, Strebel D et al., 2010. The importance of winter in annual ecosystem respiration in the High Arctic: effects of snow depth in two vegetation types. *Polar Research*, 29(1), p. 58-74. doi:10.1111/j.1751-8369.2010.00151.x

Moriana-Armendariz M, Nilsen L, Cooper E, 2022. Natural variation in snow depth and snow melt timing in the High Arctic have implications for soil and plant nutrient status and vegetation composition. *Arctic Science*, p. 1-19. doi:10.1139/as-2020-0025

Murguzur FJA, Bison M, Smis A et al., 2019. Towards a global arctic-alpine model for nearinfrared reflectance spectroscopy (NIRS) predictions of foliar nitrogen, phosphorus and carbon content. S*cientific Reports*, 9(1), p. 8259. doi: 10.1038/s41598-019-44558-9

Neby M, Semenchuk P, Neby E & Cooper E, 2021. Comparison of methods for revegetation of vehicle tracks in High Arctic tundra on Svalbard. *Arctic Science*, p.1-20. doi:10.1139/as-2021-0016

Odasz A, 1994. Nitrate reductase activity in vegetation below an arctic bird cliff, Svalbard, Norway. Journal of Vegetation *Science*, 5(6), p. 913-920. doi:10.2307/3236203

Parmentier F, Nilsen L, Tømmervik H, Cooper E, 2021. A distributed time-lapse camera network to track vegetation phenology with high temporal detail and at varying scales. *Earth System Science Data*, 13(7), pp.3593-3606. doi:10.5194/essd-13-3593-2021

Pedersen Å, Lier M, Routti H et al., 2006. Co-feeding between Svalbard Rock Ptarmigan (Lagopus muta hyperborea) and Svalbard Reindeer (Rangifer tarandus platyrhynchus). *ARCTIC*, 59(1), p. 61–64. https://doi.org/10.14430/arctic364

Richardson A D, Jenkins J P, Braswell B H et al., 2007. Use of digital webcam images to track spring green-up in a deciduous broadleaf forest. Oecologia, 152(2), p. 323–334 doi:10.1007/s00442-006-0657-z.

Richardson A, Braswell B, Hollinger D et al., 2009. Near-surface remote sensing of spatial and temporal variation in canopy phenology. *Ecological Applications*, 19(6), p. 1417-1428. doi:10.1890/08-2022.1

Robinson C, Wookey P, Lee J et al., 1998. Plant community responses to simulated environmental change at a high arctic polar semi-desert. *Ecology*, 79(3), p. 856-866. doi:10.1890/0012-9658(1998)079[0856:pcrtse]2.0.co;2

Sarwat M, 2017. Leaf senescence in plants: Nutrient remobilization and gene regulation. In: Sarwat M, Ahmad A, Abdin M & Ibrahim M, ed., *Stress signaling in plants: Genomics and proteomics perspective, Volume 2*. doi:10.1007/978-3-319-42183-4

Schaberg P, van den Berg A, Murakami P et al., 2003. Factors influencing red expression in autumn foliage of sugar maple trees. *Tree Physiology*, 23(5), p. 325-333. doi:10.1093/treephys/23.5.325

Semenchuk P, Elberling B, Amtorp C et al., 2015. Deeper snow alters soil nutrient availability and leaf nutrient status in high Arctic tundra. *Biogeochemistry*, 124(1-3), p. 81-94. doi:10.1007/s10533-015-0082-7

Semenchuk P, Gillespie M, Rumpf S et al., 2016. High Arctic plant phenology is determined by snowmelt patterns but duration of phenological periods is fixed: an example of periodicity. *Environmental Research Letters*, 11(12), p. 125006. doi:10.1088/1748-9326/11/12/125006

Sigurdsson B, 2011. Elevated CO2 and nutrient status modified leaf phenology and growth rhythm of young Populus trichocarpa trees in a 3-year field study. *Trees*, 15(7), p. 403-413 doi:10.1007/s004680100121

Strebel D, Elberling B, Morgner E et al., 2010. Cold-season soil respiration in response to grazing and warming in High-Arctic Svalbard. *Polar Research*, 29(1), p. 46-57. doi:10.1111/j.1751-8369.2010.00154.x

Street L, Mielke N & Woodin S, 2017. Phosphorus availability determines the response of tundra ecosystem carbon stocks to nitrogen enrichment. *Ecosystems*, 21(6), p. 1155-1167. doi:10.1007/s10021-017-0209-x

Sundqvist M, Moen J, Björk R et al., 2019. Experimental evidence of the long-term effects of reindeer on Arctic vegetation greenness and species richness at a larger landscape scale. *Journal of Ecology*,

107(6), p. 2724-2736.
doi:10.1111/1365-2745.13201

Thomas F, Ahlers U, 1999. Effects of excess nitrogen on frost hardiness and freezing injury of above-ground tissue in young oaks (Quercus petraea and Q. robur). *New Phytologist*, 144(1), p. 73-83. doi:10.1046/j.1469-8137.1999.00501.x

Tømmervik H, Karlsen S-R, Nilsen L et al., 2014. Use of unmanned aircraft systems (UAS) in a multi-scale vegetation index study of arctic plant communities in Adventdalen on Svalbard. *EARSeL EProceedings*, Special Issue: 34 th EARSeL Symposium. https://hdl.handle.net/10037/6651

Uchida M, Kishimoto A, Muraoka H, et al., 2010. Seasonal shift in factors controlling net ecosystem production in a High Arctic terrestrial ecosystem, *Journal of Plant Research*, 123(1), p. 79–85. doi:10.1007/s10265-009-0260-6.

Walker D A, Raynolds M K, Daniëls F J A et al., 2005. The Circumpolar Arctic Vegetation Map. *Journal of Vegetation Science*, 16(3), p. 267–282. doi:10.1111/j.1654-1103.2005.tb02365.x.

Wegener C & Odasz-Albrigtsen A, 1998. Do Svalbard reindeer regulate standing crop in the absence of predators? *Oecologia*, 116(1-2), p. 202-206. doi:10.1007/s004420050580

Westergaard-Nielsen A, Lund M, Hansen B U et al., 2013. Camera derived vegetation greenness index as proxy for gross primary production in a low arctic wetland area. *ISPRS Journal of Photogrammetry and Remote Sensing*, 86, p. 89–99. doi:10.1016/j.isprsjprs.2013.09.006.

Westergaard-Nielsen A, Lund M, Pedersen S et al., 2017. Transitions in high-Arctic vegetation growth patterns and ecosystem productivity tracked with automated cameras from 2000 to 2013. *Ambio*, 46(S1), p. 39-52. doi:10.1007/s13280-016-0864-8

Xu W, Prieme A, Cooper E et al., 2021. Deepened snow enhances gross nitrogen cycling among Pan-Arctic tundra soils during both winter and summer. *Soil Biology and Biochemistry*, 160, p. 108356. https://doi.org/10.1016/j.soilbio.2021.10835

Zhao L, Xia Y, Wu X et al., 2018. Phenotypic Analysis and Molecular Markers of Leaf Senescence. In: Guo Y, ed., *Plant Senescence: Methods and Protocols*, 1st ed. New York: Springer, p. 360. doi: https://doi.org/10.1007/978-1-4939-7672-0

Zwolicki A, Zmudczyńska-Skarbek K, Iliszko L & Stempniewicz L, 2012. Guano deposition and nutrient enrichment in the vicinity of planktivorous and piscivorous seabird colonies in Spitsbergen. *Polar Biology*, 36(3), p. 363-372. doi:10.1007/s00300-012-1265-5

Øvstedal D, Tønsberg T, Elvebakk A, 2009. The lichen flora of Svalbard. *Sommerfeltia*, 33(1), p. 3-393. doi:10.2478/v10208-011-0013-5

8 Appendix

Tables

Table T3.1: Coordinates of the nine plots.

Site #1 - *Dryas*	Site #2 - Graminoids	Site #3 - *Salix*
C1 33 X 0523835 8677644	**C2** 33 X 0524173 8677726	**C3** 33 X 0519003 8680762
W1 33 X 0523843 8677636	**W2** 33 X 0524167 8677742	**W3** 33 X 0518997 8680768
N1 33 X 0523840 8677646	**N2** 33 X 0524175 8677736	**N3** 33 X 0518988 8680756

Table T3.2: Overview of missing images for various cameras.

Camera	***Number of missing images***	***DOY***
C1	4	200, 232, 237, 240
W1	1	197
N1	5	187, 190, 197, 199, 200
C2	0	-
W2	2	255, 256
N2	0	-
C3	0	-
W3	1	239
N3	0	-

Figures

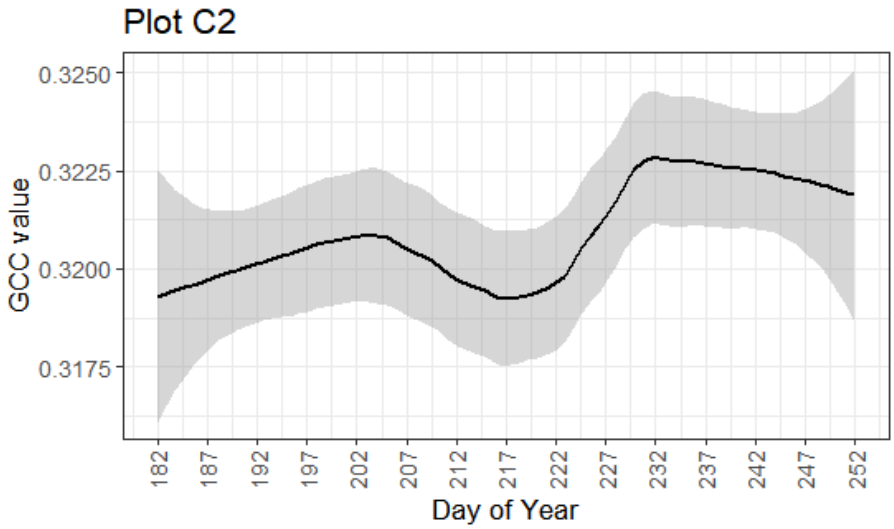

Figure A3.3: The divergent curve of the plot cameras' C2 plot. Divergent curve, low GCC value variability.

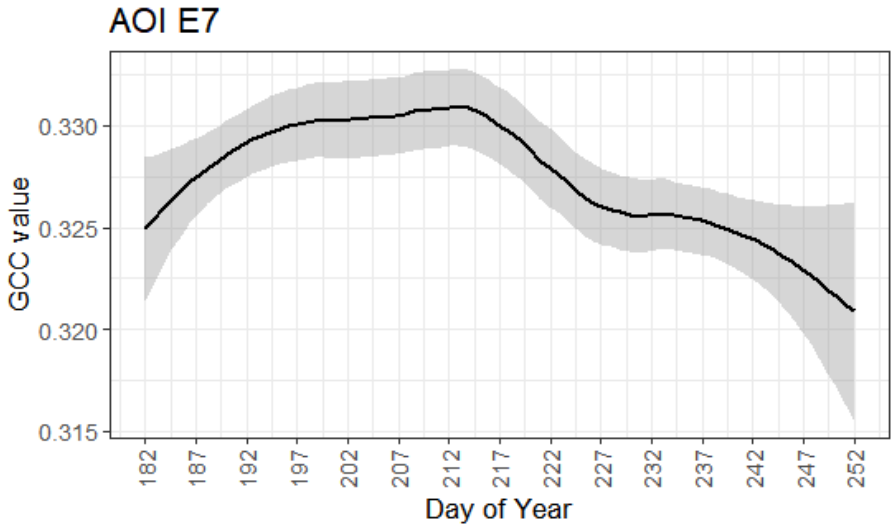

Figure A3.4: The divergent curve of the landscape camera's E7 AOI. Divergent curve, low GCC value variability.

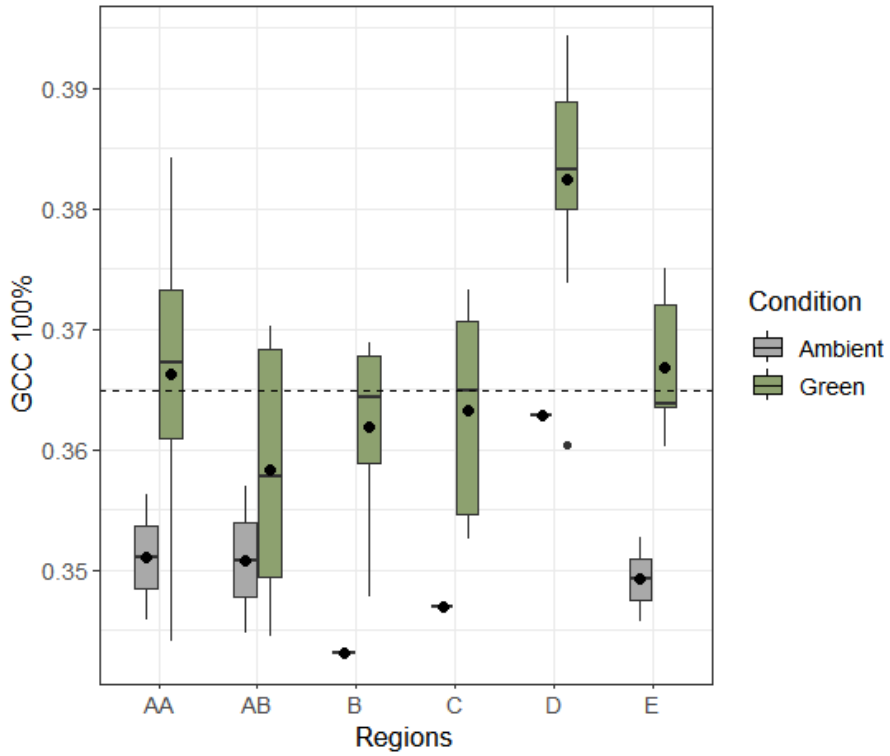

Figure A4.1: Maximum greenness level (GCC 100%) means by region and condition. Central dots indicate condition mean per region, while the dashed line marks the overall mean of the data.

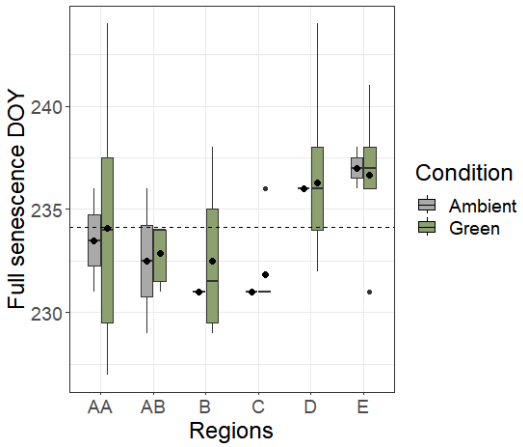

Figure A4.2: Full senescence DOY by region and condition. Central dots indicate condition mean per region, while the dashed line marks the overall mean of the data.

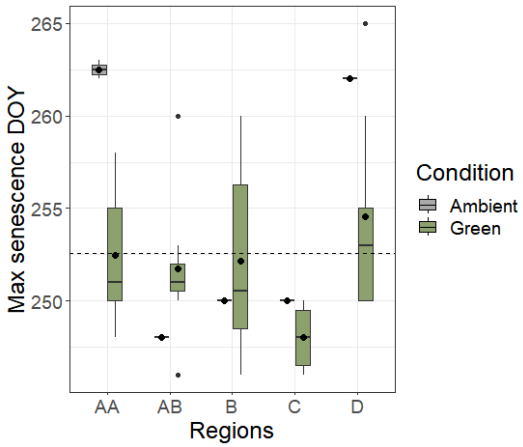

Figure A4.3: Max senescence DOY by region and condition. Central dots indicate condition mean per region, while the dashed line marks the overall mean of the data.

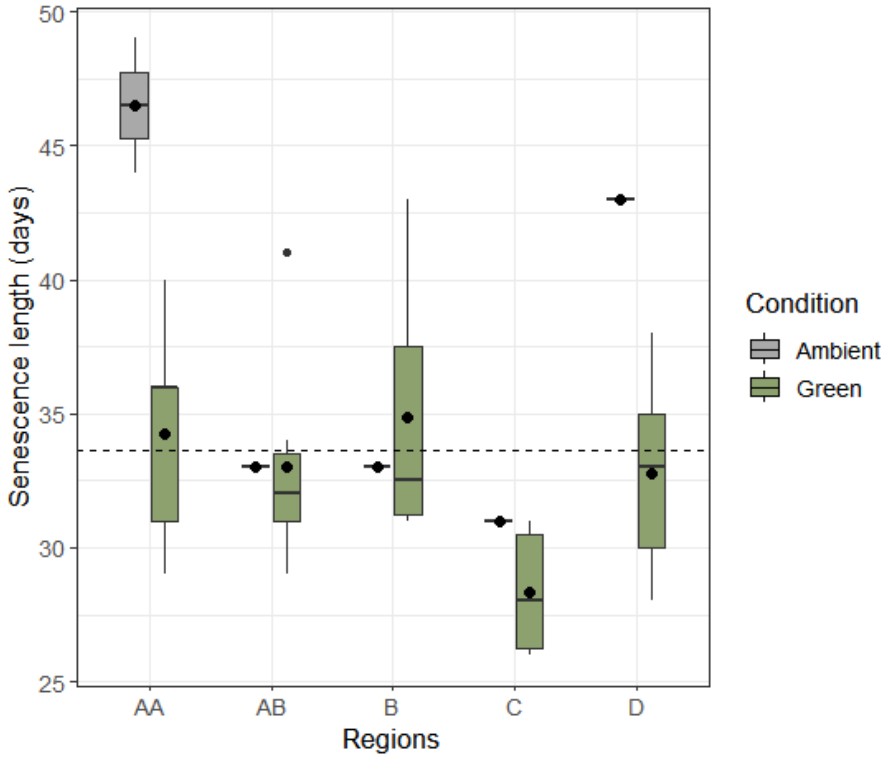

Figure A4.4: Senescence length, in days, by region and condition. Central dots indicate condition mean by region, while the dashed line marks the overall mean of the data.

R output

Table T3.1: Table for GCC model output, lm(beginning of senescence doy ~ condition + region). Regions are here named ‘subregion’ accounting for the split of region A into AA and AB.

```
Residuals:
    Min      1Q  Median      3Q     Max
-5.4326 -1.4897  0.2564  1.3121  5.4913

Coefficients:
               Estimate Std. Error t value Pr(>|t|)
(Intercept)    216.8370     0.9454 229.367  < 2e-16 ***
conditiongreen   1.5956     0.8271   1.929  0.05975 .
subregionab      0.2553     0.9895   0.258  0.79752
subregionb      -0.9189     1.0663  -0.862  0.39315
subregionc       1.3668     1.0663   1.282  0.20618
subregiond       3.0761     0.9378   3.280  0.00196 **
subregione       1.7163     1.0254   1.674  0.10083
---
Signif. codes:  0 ‘***’ 0.001 ‘**’ 0.01 ‘*’ 0.05 ‘.’ 0.1 ‘ ’ 1

Residual standard error: 2.242 on 47 degrees of freedom
Multiple R-squared:  0.3344,    Adjusted R-squared:  0.2495
F-statistic: 3.936 on 6 and 47 DF,  p-value: 0.002873
```

Table T4.1: Table for GCC model output, landscape camera, lm(beginning of senescence doy ~ gcc_100).

```
Residuals:
    Min      1Q  Median      3Q     Max 
-4.8274 -1.3919  0.1056  1.1230  6.3035 

Coefficients:
            Estimate Std. Error t value Pr(>|t|)    
(Intercept)  181.399      8.249  21.991  < 2e-16 ***
gcc_100      103.469     22.594   4.579 2.94e-05 ***
---
Signif. codes:  0 ‘***’ 0.001 ‘**’ 0.01 ‘*’ 0.05 ‘.’ 0.1 ‘ ’ 1

Residual standard error: 2.205 on 52 degrees of freedom
Multiple R-squared:  0.2874,    Adjusted R-squared:  0.2737 
F-statistic: 20.97 on 1 and 52 DF,  p-value: 2.942e-05
```

Table T4.2: Table for GCC model output, landscape camera, lm(beginning of senescence doy ~ condition).

```
Residuals:
    Min      1Q  Median      3Q     Max 
-6.4444 -2.0000  0.0556  1.3333  7.5556 

Coefficients:
               Estimate Std. Error t value Pr(>|t|)    
(Intercept)    217.6667     0.8411 258.778   <2e-16 ***
conditiongreen   1.7778     0.9214   1.929   0.0591 .  
---
Signif. codes:  0 ‘***’ 0.001 ‘**’ 0.01 ‘*’ 0.05 ‘.’ 0.1 ‘ ’ 1

Residual standard error: 2.523 on 52 degrees of freedom
Multiple R-squared:  0.06681,   Adjusted R-squared:  0.04886 
F-statistic: 3.723 on 1 and 52 DF,  p-value: 0.05915
```

Table T4.3: Table for GCC model output, plots, lm(beginning of senescence doy ~ gcc_100).

```
Residuals:
       1        2        3        5        7        8        9
 -2.1969  12.4709  -9.3792  13.0331   0.2171  -3.6040 -10.5410


Coefficients:
            Estimate Std. Error t value Pr(>|t|)
(Intercept)   -148.8      100.4  -1.481   0.1986
gcc_100        902.9      249.0   3.627   0.0151 *
---
Signif. codes:  0 ‘***’ 0.001 ‘**’ 0.01 ‘*’ 0.05 ‘.’ 0.1 ‘ ’ 1


Residual standard error: 10.41 on 5 degrees of freedom
  (2 observations deleted due to missingness)
Multiple R-squared:  0.7245,    Adjusted R-squared:  0.6695
F-statistic: 13.15 on 1 and 5 DF,  p-value: 0.01512
```

Table T4.4A: Table for GCC model output, landscape camera, lm(growing season length ~ active snowmelt doy).

```
Residuals:
    Min      1Q  Median      3Q     Max
-6.8166 -2.2671  0.3299  2.7503  6.6486

Coefficients:
            Estimate Std. Error t value Pr(>|t|)
(Intercept) 180.9334    16.9120  10.699 9.59e-15 ***
as_doy_gcc   -0.8535     0.1069  -7.986 1.34e-10 ***
---
Signif. codes:  0 ‘***’ 0.001 ‘**’ 0.01 ‘*’ 0.05 ‘.’ 0.1 ‘ ’ 1

Residual standard error: 3.407 on 52 degrees of freedom
Multiple R-squared:  0.5509,    Adjusted R-squared:  0.5422
F-statistic: 63.78 on 1 and 52 DF,  p-value: 1.34e-10
```

Table T4.4B: Table for GCC model output, landscape camera, lm(gcc_100 ~ active snowmelt doy).

```
Residuals:
       Min         1Q     Median         3Q        Max
-0.0252815 -0.0059942 -0.0001748  0.0062302  0.0209141

Coefficients:
              Estimate Std. Error t value Pr(>|t|)
(Intercept) -0.0056702  0.0432668  -0.131    0.896
as_doy_gcc   0.0023422  0.0002734   8.566 1.64e-11 ***
---
Signif. codes:  0 ‘***’ 0.001 ‘**’ 0.01 ‘*’ 0.05 ‘.’ 0.1 ‘ ’ 1

Residual standard error: 0.008716 on 52 degrees of freedom
Multiple R-squared:  0.5853,    Adjusted R-squared:  0.5773
F-statistic: 73.38 on 1 and 52 DF,  p-value: 1.638e-11
```

Table T4.5A: Table for GCC model output, plots, lm(beginning of senescence doy ~ site). Site is in the model named 'sname'.

```
Residuals:
         1          2          3          5          7          8          9
-4.000e+00  2.000e+00  2.000e+00 -2.220e-16 -2.333e+00  6.667e+00 -4.333e+00

Coefficients:
                Estimate Std. Error t value Pr(>|t|)
(Intercept)      228.000      2.779  82.047 1.32e-07 ***
snamegraminoids    5.000      5.558   0.900  0.41918
snamesalix       -31.667      3.930  -8.058  0.00129 **
---
Signif. codes:  0 '***' 0.001 '**' 0.01 '*' 0.05 '.' 0.1 ' ' 1

Residual standard error: 4.813 on 4 degrees of freedom
  (2 observations deleted due to missingness)
Multiple R-squared:  0.9529,    Adjusted R-squared:  0.9294
F-statistic: 40.49 on 2 and 4 DF,  p-value: 0.002215
```

Table T4.5B: Table for NDVI model output, plots, lm(beginning of senescence doy ~ site). Site is in the model named 'sname'.

```
Residuals:
     Min       1Q   Median       3Q      Max
-11.3333  -0.6667   0.3333   5.3333   5.6667

Coefficients:
                Estimate Std. Error t value Pr(>|t|)
(Intercept)      223.333      3.859  57.879 1.79e-09 ***
snamegraminoids    7.333      5.457   1.344   0.2276
snamesalix       -19.667      5.457  -3.604   0.0113 *
---
Signif. codes:  0 '***' 0.001 '**' 0.01 '*' 0.05 '.' 0.1 ' ' 1

Residual standard error: 6.683 on 6 degrees of freedom
Multiple R-squared:  0.8136,    Adjusted R-squared:  0.7514
F-statistic: 13.09 on 2 and 6 DF,  p-value: 0.006479
```

Table T4.6: Table for GCC model, plots, lm(fs_doy_gcc ~ ndiff). Ndiff is the difference in N content at the plots at the end of field work, DOY 198.

```
Residuals:
   Min     1Q Median     3Q    Max
-4.713 -3.347 -1.123  3.005  6.773

Coefficients:
             Estimate Std. Error t value Pr(>|t|)
(Intercept) 2.315e+02  1.659e+00 139.487 9.16e-12 ***
ndiff       2.603e-03  1.032e-03   2.521   0.0452 *
---
Signif. codes:  0 ‘***’ 0.001 ‘**’ 0.01 ‘*’ 0.05 ‘.’ 0.1 ‘ ’ 1

Residual standard error: 4.552 on 6 degrees of freedom
  (1 observation deleted due to missingness)
Multiple R-squared:  0.5144,    Adjusted R-squared:  0.4335
F-statistic: 6.356 on 1 and 6 DF,  p-value: 0.04522
```

Table T4.7: Table for GCC model, plots, lm(fs_doy_gcc ~ ldiff). Ldiff is the difference in LOI content at the plots at the end of field work, DOY 198.

```
Residuals:
   Min     1Q Median     3Q    Max
-4.713 -3.347 -1.123  3.005  6.773

Coefficients:
             Estimate Std. Error t value Pr(>|t|)
(Intercept) 2.315e+02  1.659e+00 139.487 9.16e-12 ***
ndiff       2.603e-03  1.032e-03   2.521   0.0452 *
---
Signif. codes:  0 ‘***’ 0.001 ‘**’ 0.01 ‘*’ 0.05 ‘.’ 0.1 ‘ ’ 1

Residual standard error: 4.552 on 6 degrees of freedom
  (1 observation deleted due to missingness)
Multiple R-squared:  0.5144,    Adjusted R-squared:  0.4335
F-statistic: 6.356 on 1 and 6 DF,  p-value: 0.04522
```

Table T4.8A: Table for GCC model, plots, lm(ms_doy_gcc ~ p_st), peak soil temperature.

```
Residuals:
       1        2        3        5        6        7        8
 2.35031  2.89403  2.89403 -0.05543 -0.21663 -5.68657 -2.17974

Coefficients:
            Estimate Std. Error t value Pr(>|t|)
(Intercept)  274.286     11.920  23.010 2.88e-06 ***
p_st          -3.456      1.274  -2.713   0.0421 *
---
Signif. codes:  0 ‘***’ 0.001 ‘**’ 0.01 ‘*’ 0.05 ‘.’ 0.1 ‘ ’ 1

Residual standard error: 3.447 on 5 degrees of freedom
  (2 observations deleted due to missingness)
Multiple R-squared:  0.5954,    Adjusted R-squared:  0.5145
F-statistic: 7.359 on 1 and 5 DF,  p-value: 0.04214
```

Table T4.8B: Table for NDVI model, plots, lm(ms_doy_ndvi ~ p_st), peak soil temperature.

```
Residuals:
    Min      1Q  Median      3Q     Max
-4.4372 -2.4943 -0.4981  1.3991  6.9994

Coefficients:
            Estimate Std. Error t value Pr(>|t|)
(Intercept)  279.985     13.981  20.027 1.01e-06 ***
p_st          -4.061      1.511  -2.688   0.0362 *
---
Signif. codes:  0 ‘***’ 0.001 ‘**’ 0.01 ‘*’ 0.05 ‘.’ 0.1 ‘ ’ 1

Residual standard error: 4.241 on 6 degrees of freedom
  (1 observation deleted due to missingness)
Multiple R-squared:  0.5463,    Adjusted R-squared:  0.4707
F-statistic: 7.224 on 1 and 6 DF,  p-value: 0.03616
```

Table T4.8C: Table for GCC model, plots, lm(ms_doy_gcc ~ mean_st), mean soil temperature.

```
Residuals:
      1       2       3       5       6       7       8
 2.6521  2.3222  1.9286 -0.2950  0.9392 -4.5181 -3.0289

Coefficients:
            Estimate Std. Error t value Pr(>|t|)
(Intercept)  290.583     14.838  19.584 6.41e-06 ***
mean_st       -7.873      2.404  -3.275   0.0221 *
---
Signif. codes:  0 ‘***’ 0.001 ‘**’ 0.01 ‘*’ 0.05 ‘.’ 0.1 ‘ ’ 1

Residual standard error: 3.056 on 5 degrees of freedom
  (2 observations deleted due to missingness)
Multiple R-squared:  0.682,     Adjusted R-squared:  0.6184
F-statistic: 10.72 on 1 and 5 DF,  p-value: 0.02209
```

Table T4.8D: Table for NDVI model, plots, lm(ms_doy_ndvi ~ mean_st), mean soil temperature.

```
Residuals:
    Min      1Q  Median      3Q     Max
-5.6168 -2.0902 -0.1309  2.0441  6.1408

Coefficients:
            Estimate Std. Error t value Pr(>|t|)
(Intercept)  299.221     19.287  15.514 4.54e-06 ***
mean_st       -9.234      3.138  -2.942   0.0259 *
---
Signif. codes:  0 ‘***’ 0.001 ‘**’ 0.01 ‘*’ 0.05 ‘.’ 0.1 ‘ ’ 1

Residual standard error: 4.028 on 6 degrees of freedom
  (1 observation deleted due to missingness)
Multiple R-squared:  0.5907,    Adjusted R-squared:  0.5224
F-statistic: 8.658 on 1 and 6 DF,  p-value: 0.02586
```

Table T4.9: Table for GCC model, plots, lm(ms_doy_gcc ~ ndiff). Ndiff is the difference in N content at the plots at the end of field work, DOY 198.

```
Residuals:
    Min      1Q  Median      3Q     Max
-4.1520 -1.4684  0.3794  1.6687  3.8285

Coefficients:
             Estimate Std. Error t value Pr(>|t|)
(Intercept) 2.412e+02  1.048e+00 230.098 4.55e-13 ***
ndiff       2.237e-03  6.522e-04   3.429    0.014 *
---
Signif. codes:  0 ‘***’ 0.001 ‘**’ 0.01 ‘*’ 0.05 ‘.’ 0.1 ‘ ’ 1

Residual standard error: 2.876 on 6 degrees of freedom
  (1 observation deleted due to missingness)
Multiple R-squared:  0.6622,    Adjusted R-squared:  0.6059
F-statistic: 11.76 on 1 and 6 DF,  p-value: 0.01398
```

Table T4.10: Table for GCC model, plots, lm(ms_doy_gcc ~ ldiff). Ldiff is the difference in LOI content at the plots at the end of field work, DOY 198.

```
Residuals:
    Min      1Q  Median      3Q     Max
-5.4266 -1.5323  0.2932  2.2090  3.3383

Coefficients:
            Estimate Std. Error t value Pr(>|t|)
(Intercept) 241.3658     1.1315 213.307 7.16e-13 ***
ldiff         0.4241     0.1407   3.014   0.0236 *
---
Signif. codes:  0 ‘***’ 0.001 ‘**’ 0.01 ‘*’ 0.05 ‘.’ 0.1 ‘ ’ 1

Residual standard error: 3.12 on 6 degrees of freedom
  (1 observation deleted due to missingness)
Multiple R-squared:  0.6023,    Adjusted R-squared:  0.536
F-statistic: 9.086 on 1 and 6 DF,  p-value: 0.02357
```

Table T4.11: Table for GCC model, plots, lm(sen_length_gcc ~ gcc_100).

```
Residuals:
      1       2       3       5       7       8       9
 -1.719 -10.772   7.008  -6.789  -5.096   4.337  13.031


Coefficients:
            Estimate Std. Error t value Pr(>|t|)
(Intercept)    322.9       89.3   3.616   0.0153 *
gcc_100       -734.7      221.4  -3.319   0.0210 *
---
Signif. codes:  0 ‘***’ 0.001 ‘**’ 0.01 ‘*’ 0.05 ‘.’ 0.1 ‘ ’ 1


Residual standard error: 9.261 on 5 degrees of freedom
  (2 observations deleted due to missingness)
Multiple R-squared:  0.6878,    Adjusted R-squared:  0.6254
F-statistic: 11.02 on 1 and 5 DF,  p-value: 0.02103
```